Volume 7 | Number 10 | October 2014 | Pages 3089–3444

# Energy & Environmental Science

www.rsc.org/ees

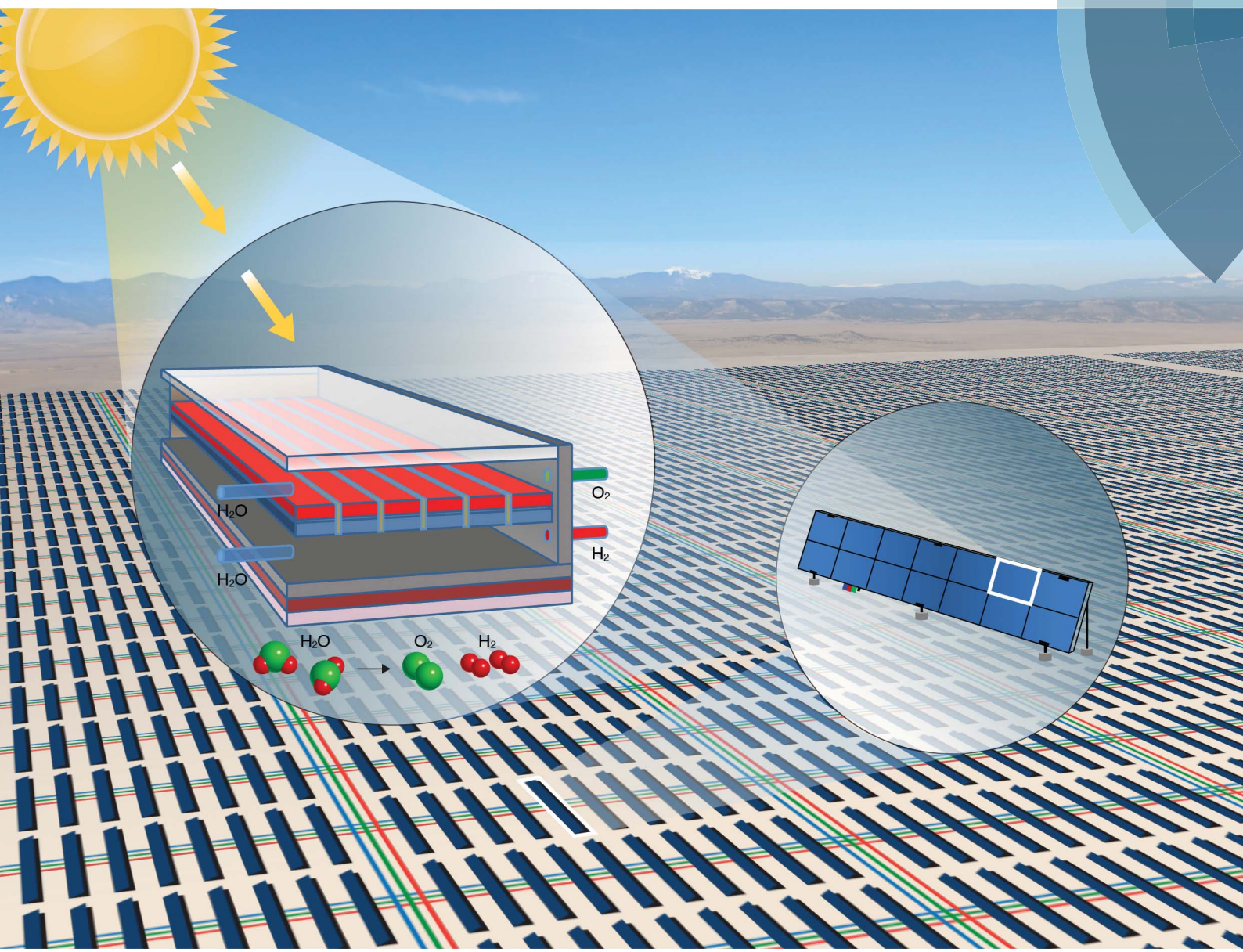


ISSN 1754-5692

ROYAL SOCIETY OF CHEMISTRY

ANALYSIS

Roger Sathre, Jeffery B. Greenblatt *et al.*

Life-cycle net energy assessment of large-scale hydrogen production *via* photoelectrochemical water splitting

Energy & Environmental Science

ANALYSIS

View Article Online
View Journal | View Issue



Cite this: *Energy Environ. Sci.*, 2014, **7**, 3264

# Life-cycle net energy assessment of large-scale hydrogen production *via* photoelectrochemical water splitting†

Roger Sathre,*[ab] Corinne D. Scown,[ab] William R. Morrow, III,[ab] John C. Stevens,[ac] Ian D. Sharp,[ad] Joel W. Ager, III,[ac] Karl Walczak,[ac] Frances A. Houle[ae] and Jeffery B. Greenblatt*[ab]

Received 1st April 2014
Accepted 16th June 2014

DOI: 10.1039/c4ee01019a

www.rsc.org/ees



Here we report a prospective life-cycle net energy assessment of a hypothetical large-scale photoelectrochemical (PEC) hydrogen production facility with energy output equivalent to 1 GW continuous annual average (1 GW HHV = 610 metric tons of $H_2$ per day). We determine essential mass and energy flows based on fundamental principles, and use heuristic methods to conduct a preliminary engineering design of the facility. We then develop and apply a parametric model describing system-wide energy flows associated with the production, utilization, and decommissioning of the facility. Based on these flows, we calculate and interpret life-cycle net energy metrics for the facility. We find that under base-case conditions the energy payback time is 8.1 years, the energy return on energy invested (EROEI) is 1.7, and the life-cycle primary energy balance over the 40 years projected service life of the facility is +500 PJ. The most important model parameters affecting the net energy metrics are the solar-to-hydrogen (STH) conversion efficiency and the life span of the PEC cells; parameters associated with the balance of systems (BOS), including construction and operation of the liquid and gas handling infrastructure, play a much smaller role.

**Broader context**

The use of sunlight to generate carbon-neutral fuels for transportation and feedstocks offers the possibility of widespread sources of environmentally benign, energy rich chemicals across the globe. Although still at an early stage, there is sufficient information about using sunlight and water to make hydrogen, which can be used directly in fuel cells and as feedstock for production of liquid hydrocarbon fuels, to perform an assessment of whether its large scale production would be advantageous from a net energy production point of view. This assessment is performed by building a reasonable scenario for a solar hydrogen production facility, and determining the energy costs to build, operate, and decommission it. In this work we have determined that such a plant can be energy-positive; however, the hydrogen-generating devices must meet certain efficiency and durability criteria. This result suggests that a strong program of research into improved materials and methods to process the materials will have a high impact on the feasibility of this technology.

## 1. Introduction

To reduce dependence on fossil fuels and achieve substantial greenhouse gas (GHG) emissions reductions, humans must harness renewable energy.[1] Wind turbines, biofuels and photovoltaic (PV) panels are, at a fundamental level, mechanisms for converting the sun's energy into useful power. For example, PV panels convert solar energy to electricity at efficiencies ranging from below 10% to over 20%, with new solar cells achieving above 40% conversion efficiency under laboratory conditions.[2] Because these renewable energy sources are inherently intermittent over diurnal and annual cycles and are not necessarily aligned with patterns of human energy demand, great value is placed on renewable energy technologies capable of providing forms of energy that are easily stored. Large-scale electricity storage remains costly, with energy losses of 20–30% for pumped hydro or compressed air storage.[3] Biofuel crops can be used to produce a variety of fuels but convert solar energy to biomass at efficiencies below 1%, not including the energy used during harvest, transportation, and conversion.[4] Despite the relatively low conversion efficiency of bioenergy, it remains a

[a]*Joint Center for Artificial Photosynthesis, Berkeley CA, USA. E-mail: rsathre@lbl.gov; jbgreenblatt@lbl.gov*

[b]*Environmental Energy Technologies Division, Lawrence Berkeley National Laboratory, Berkeley CA, USA*

[c]*Materials Sciences Division, Lawrence Berkeley National Laboratory, Berkeley CA, USA*

[d]*Physical Biosciences Division, Lawrence Berkeley National Laboratory, Berkeley CA, USA*

[e]*Chemical Sciences Division, Lawrence Berkeley National Laboratory, Berkeley CA, USA*

† Electronic supplementary information (ESI) available. See DOI: 10.1039/c4ee01019a

competitive technology because liquid biofuels are energy-dense and, unlike electricity, easily stored.[5]

The goal of current photoelectrochemical (PEC) water splitting technology is to directly convert solar radiation to a storable fuel – hydrogen – at solar energy conversion efficiencies many times greater than natural photosynthesis.[6] More advanced PEC cells may eventually be capable of reducing $CO_2$, which would provide a route to hydrocarbon synfuel production.[7] PEC water splitting involves the use of semiconductor absorbers in combination with catalysts to generate $H_2$, as well as $O_2$ as a by-product, using sunlight and water as inputs.[8] Here, we consider systems that operate spontaneously, without the need for external electrical bias. Laboratory demonstrations have achieved solar-to-hydrogen (STH) efficiencies in the 5–18% range,[9–15] and ongoing research aims to improve performance, increase lifetime and reduce cost to allow eventual large-scale implementation.[16–20]

If produced from sustainable resources such as solar energy and water, hydrogen can play an important role in an eventual sustainable economy because it offers a carbon-free, high energy-density, versatile fuel that can be used directly in fuel cells for stationary power generation or vehicle powertrains,[21] as well as industrial applications including fuel upgrading or Fischer–Tropsch synfuel production.[22] As of 2006, global hydrogen production totaled 48 million metric tons (Mt) per year, with 20 Mt produced in the United States (US).[23] Most hydrogen is currently produced by steam methane reforming, with smaller amounts produced using electrolyzers or as a by-product of industrial processes. Of total US hydrogen production, 64% was consumed for petroleum refining and 33% went to chemicals production (primarily ammonia production). Global estimates indicate a potential demand of 300 Mt $H_2$ per year in 2050,[24] with an energy equivalent of roughly 1.1 trillion liters of gasoline. For comparison, the world consumed 5.3 trillion liters of liquid fuels in 2013.[25] Given the projected US share of global liquid fuel demand, the US would be responsible for 20% of global $H_2$ demand, or 60 Mt $H_2$ per year.

While solar-to-hydrogen technologies are currently far less developed than other solar-to-fuel routes such as biofuels, prospective modeling of such systems provides insight into their potential competitiveness and helps to identify key challenges and opportunities for improvement. Initial techno-economic analysis of solar PEC $H_2$ generation has been performed by James *et al.*[26] and Pinaud *et al.*[27] These pioneering studies described four different configurations of PEC devices, including a flat plate collector, a concentrating collector, and two variations of colloidal suspensions of PEC nanoparticles. These studies explored the practical landscape of PEC scale-up, comparing economic metrics of PEC $H_2$ generation. To date, however, the literature contains limited analysis of the energetic metrics of PEC $H_2$. Net energy analysis provides a fundamental basis of comparison for all energy technologies, particularly for renewable-based energy and their contribution towards sustainability. The net energy of a system is the energy available for societal use, after subtracting the energy required to produce and operate the technology. If the energy inputs to the system approach or exceed the solar energy harvested by the system, its contribution to sustaining societal wellbeing becomes negligible. In this context, it is important to evaluate the primary energy costs associated with solar-to-fuels technologies to determine a baseline for viability and to identify specific component or system level energy costs that may constrain future implementation. Thus, prospective life-cycle system modeling can produce insights that may guide fundamental research and stimulate effective innovation in the most critical areas.

Previous analysis has described the net energy balance of an individual PEC cell including photoelectrodes, catalysts, and encapsulation.[28] However, the energy implications of balance-of-systems (BOS) requirements of a PEC $H_2$ production facility have not been analyzed heretofore. The BOS of a complete PEC $H_2$ production facility includes all components beyond the actual PEC cells, such as structural supports, manifolds and pipes, pumps, compressors, storage tanks, pipelines, roads and monitoring systems. The objective of this study is to identify and credibly estimate the life-cycle energy flows associated with a projected large-scale PEC $H_2$ production system, including PEC cells and BOS components and processes. We then analyze the life-cycle net energy implications of the system under varying levels of projected performance in terms of *e.g.*, efficiency and durability. Because prospective analysis of early-stage technologies is inherently uncertain, we focus on identifying the sources and magnitudes of significant uncertainties, and their effects on the net energy results, to guide future research and development priorities.

## 2. Methods

### 2.1 Modeling approach

We use prospective life-cycle assessment (LCA), a method for quantifying cradle-to-grave environmental and/or economic impacts of a product or service, to estimate the net energy implications of a hypothetical large-scale PEC hydrogen production facility. Specifically, prospective LCA is a method for combining scenario analysis with consequential LCA to assess the potential impacts of technologies and infrastructure systems that are not yet operating at commercial scale.[29]

Our large-scale PEC hydrogen production scenario is based on a hypothetical PEC facility with $H_2$ production equivalent to 1 GW annual average (1 GW HHV annual average = 610 t $H_2$ per day = 6.8 million $Nm^3$ per day).‡ We apply fundamental principles such as mass and energy balance to determine essential flows. Next, we conduct a preliminary engineering design of the facility, based on heuristic methods. We then develop and apply a parametric model describing system-wide energy flows associated with the production, utilization, and decommissioning of the facility. Based on these flows, we calculate three net energy metrics for the facility.

‡ The annual $H_2$ production of the modeled facility corresponds to 1 GW continuous power output, averaged across diurnal and seasonal cycles. 1 GW continuous power for one year is equivalent to 31.5 PJ of energy. Peak $H_2$ production rate in full sunlight is 3.6 times the average output rate. $Nm^3$ is normal cubic meters, at 20 °C temperature and 1 atm pressure.

The *life-cycle primary energy balance* describes how much usable energy the facility provides to society during its life span. In units of PJ, it is calculated as the total energy output minus the total energy input:

$$\text{Energy balance} = \{T \times E_H\} - \{E_P + (T \times E_O) + E_D\}$$

where $T$ = service life of the facility (years).

$E_H$ = energy (HHV) in hydrogen produced in 1 year (PJ per year).

$E_P$ = energy used to produce the facility (PJ).

$E_O$ = energy used to operate the facility for 1 year (PJ per year).

$E_D$ = energy used to decommission the facility (PJ).

The *energy return on energy invested* (EROEI, sometimes denoted as EROI) describes how much usable energy the facility will deliver, relative to its required energy inputs. A value without units, it is calculated as the total energy output divided by the total energy input:

$$\text{EROEI} = \frac{T \times E_H}{E_P + (T \times E_O) + E_D}$$

The *energy payback time* describes how long the facility must operate for it to deliver the $H_2$ equivalent of the energy required for its manufacturing, construction, and decommissioning. Note that energy payback time is not a life-cycle metric as it does not consider the energy that continues to be delivered after the payback time is reached; the equation does not include the variable $T$, the facility service life. In units of years, it is calculated as the fixed energy inputs divided by the annual net energy output under full scale steady state operation:

$$\text{Energy payback time} = \frac{E_P + E_D}{E_H - E_O}$$

Acknowledging the inherent uncertainties of future projections, our primary goals are to bound the solution space and identify sources of significant variation. Our system model includes base-case values for each parameter, as well as low and high values indicative of current uncertainty regarding the actual value of the parameters in a future large-scale physical system. Parameter valuation is based on literature review, proxy data on analogous processes, and informed estimates. Low, base-case and high values of system parameters are listed in Table S1.† Low values correspond to reduced system performance relative to the base-case, while high values correspond to improved performance. We conduct a sensitivity analysis by varying individual parameters one at a time between low and high values. Within parameter categories, we also conduct Monte Carlo simulations to estimate uncertainty introduced by interactions between individual parameters. Simulation was conducted using Oracle® Crystal Ball software. Triangular probability distributions were assumed for each parameter based on low, base-case and high values (Table S1†). Based on the outcome distribution of 10 000 simulations of each category grouping, 90% confidence intervals were determined and displayed as error bars on results figures. Outcomes of the Monte Carlo simulations are shown in Fig. S1.†

We consider two forms of energy used to construct and operate the facility: fossil fuels and electricity. Comprehensive energy accounting must be done using comparable units, thus different energy carriers and end-uses are generally considered in terms of their "primary energy" use. Primary energy is in a form found in nature, prior to any conversion or transformation process. For raw fossil fuels, their primary energy is defined by their heat content. For other derived energy carriers, such as electricity and refined fuels, primary energy includes all energy used upstream for *e.g.* extraction, transportation, processing, conversion and distribution of the energy carriers. For diesel fuel used in the facility, we estimate its primary energy as the higher heating value (HHV) of the fuel plus 13% fuel cycle inputs.[30] The primary energy of electricity depends on how it is generated; for example, electricity from a coal-fired power plant typically has a primary energy conversion efficiency of about 33%, meaning that about 3 J of primary energy are needed for each J of electricity produced. Estimating the primary energy of non-thermal electricity sources, such as hydroelectric and PV, is less straightforward.[31] Furthermore, a particular challenge in performing prospective energy analysis is to estimate primary energy use associated with future electricity generation, for example the electricity used to operate the $H_2$ production facility modeled here.

In this analysis, the electricity required for on-site operational needs (*e.g.* gas handling equipment, electronic monitoring) is assumed to be generated externally and provided as an input to the facility from the electricity grid. Grid electricity, which comes from a range of fossil and renewable sources, is likely to change markedly in composition over the next several decades. We consider the hydrogen gas produced by the facility as primary energy, equivalent to its higher heating value. We convert end-use electricity to primary energy, assuming a conversion efficiency of 50% based on current $H_2$ fuel cell performance.[32] In other words, we estimate the primary energy of electricity inputs to the facility, as if that electricity were produced from the hydrogen made by the facility. We use this energy accounting technique merely to derive comparable primary energy values for different energy carriers; all the $H_2$ produced is actually delivered for external use, and electricity is a separate input to the facility. Despite the modest electrical requirements of the system, the impact on total net primary energy is sensitive to this choice, which we explore in a sensitivity analysis.

Our modeling encompasses the short-term dynamics of diurnal and seasonal variation in solar radiation, as well as long-term dynamics of life-cycle phases including facility manufacture, operation, maintenance and replacement, and end-of-life disposal. We distinguish between service life spans of PEC cells (base case: 10 years until replacement) and balance of system (base case: 40 years until decommissioning). We use a simplified approach to account for the shorter service life of PEC cells, by assuming steady-state conditions in which a fixed percentage of panels are replaced each year. For cells with a 10 year life span, we assume that 10% of the panels are replaced annually, which implicitly assumes a phased facility construction in which 10% of the panels are put into service during each

 

of the first 10 years. We do not model this facility ramp-up period, but instead base our calculations on eventual steady-state conditions. We further assume that cell performance degrades linearly over time, with panel replacement occurring when STH efficiency falls to 80% of its original value. This is implemented in the model through a simple "degradation factor" such that the average $H_2$ production over the life span of a panel corresponds to 90% of the nominal STH efficiency. If continuing technological progress allows higher STH efficiencies in the future, it may be possible to replace degraded panels with new panels of higher efficiency. This would improve overall efficiency of the facility, though the level of improvement would ultimately be constrained by the capacity of the balance of system of the facility. We did not model changes in STH efficiency over time, and within each STH efficiency scenario we assume that panels are replaced by new panels of the same efficiency.

### 2.2 Facility description

We consider a solar-to-hydrogen (STH) efficiency of 10% as a base case, as there have been a number of demonstrations of PEC devices operating at or above this value. We define the STH efficiency as suggested by Chen *et al.*,[33] based on the Gibbs free energy§ of the $H_2$ produced under AM1.5G solar radiation. We assume a linear relation between instantaneous radiation and $H_2$ production (see Fig. S7†), acknowledging that variations in efficiency will exist in practice.[34] We assume 10% solar transmittance loss due to the combined effects of absorption and reflection by surface dust, encapsulation material, and electrolyte.

The hydrogen production facility is configured on four hierarchical levels (Fig. 1). From smaller to larger, these are: (1) a PEC "cell" of ~2 $m^2$; (2) a truck-transportable "panel" of ~29 $m^2$ comprising multiple cells; (3) a "field" of 1000 panels plus gas compression and storage, occupying 12 ha; and (4) the 1 GW (continuous annual average) "facility" of 1510 fields occupying 180 $km^2$ of land in the base-case of 10% STH efficiency. The fixed flat panel array format is similar to the Type 3 PEC design described in the technoeconomic analysis by James *et al.*[26] and Pinaud *et al.*,[27] though both the panel size and facility size are larger in our life-cycle net energy analysis. We have chosen to model the flat panel format (Type 3) because it is at a more mature developmental stage than alternatives including colloidal suspension reactors (Types 1 and 2) and tracking concentrating systems (Type 4).

A "cell" comprises the fundamental components required for unassisted solar water splitting. These include semiconductors that absorb solar radiation, coupled to catalysts for oxygen and hydrogen evolution reactions. A membrane is integrated into the cell to ensure that combustible gas product mixtures are not generated and to enable ionic transport from the region of oxygen evolution to the region of hydrogen evolution. The complete assembly is immersed in electrolyte and enclosed in a chassis with an input for liquid water and

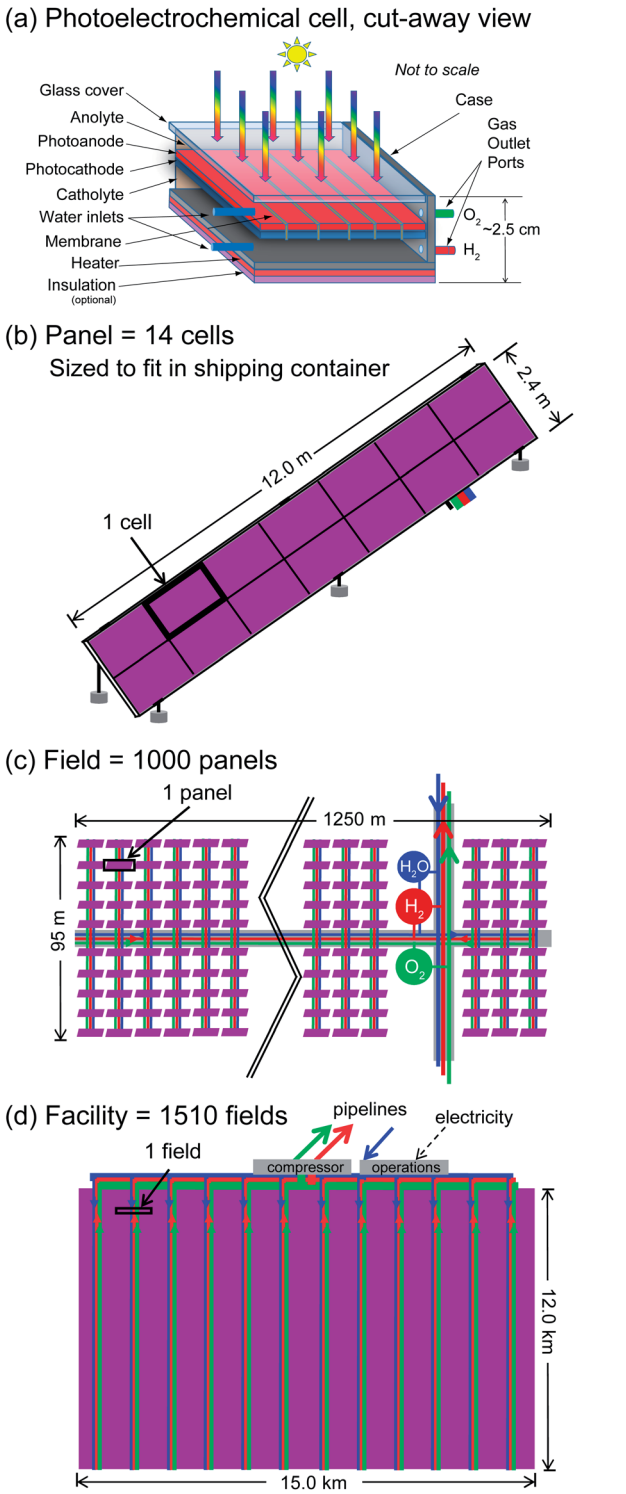


Fig. 1 Four hierarchical levels of the 1 GW (continuous annual average) hydrogen production facility. The full size of the PEC cell, shown partially in cut-away view, is 1.7 m × 1.2 m.

§ STH efficiency is defined in terms of Gibbs free energy of $H_2$, per the convention in the PEC community.[33] We define our 1 GW facility based on the higher heating value (HHV) of $H_2$, because HHV is an energy measurement convention commonly used in US energy system analysis. Our analysis applies appropriate conversion factors. One mole of $H_2$ has Gibbs free energy of 237.1 kJ, lower heating value (LHV) of 242.3 kJ, and HHV of 286.6 kJ.

separate outputs for gaseous oxygen and hydrogen. No external electricity is used in the PEC cells for water splitting.

A "panel" is 12.0 m long by 2.4 m wide, and includes a structural frame upon which multiple PEC cells are mounted (see Fig. S2†). Panels include onboard monitoring and diagnostics sensors, and pipe manifolds for transferring fluids to and from each cell. Panels have standardized fluid and data connections so they can be installed and removed from the facility relatively easily. The total weight of a panel is about 720 kg without electrolyte and 1300 kg including electrolyte. More details of panels are listed in Table S2.†

A "field" comprises 1000 panels plus compression and storage infrastructure for one day's production of $H_2$ (see Fig. S3†). The panels are tilted towards the equator at an angle equal to the local latitude, here assumed to be 34°. Spacing between panels is assumed to be 0.5 m end-to-end. Spacing between rows of panels determines losses due to shading by adjacent panels when the sun is low in the sky. Following James *et al.*[26] and Pinaud *et al.*,[27] we have determined spacing between the rows of panels based on a 10° shading angle (see Fig. S4†). We have not attempted to optimize panel spacing, nor have we analyzed whether the approach to gas compression used here, *i.e.* parallel compression in each of the 1000 fields, is more or less efficient than other possible approaches, *e.g.*, compression and storage with fewer, larger-scale compressors and tanks.

The entire "facility" aggregates production from 1510 fields, with a 90% capacity factor (*i.e.* 90% of the panels are producing $H_2$ on an average day) (see Fig. S5†). The facility is assumed to be located in the southwest US. Solar resource data are taken from NREL,[35] and are the average of monthly mean flat-panel insolation at four sites: Phoenix, Daggett, Tucson and Las Vegas (see Fig. S6†). The annual average solar insolation is 276 W $m^{-2}$.

The intermittency of solar resource is addressed through distributed compression and storage of $H_2$. Pre-compression gas conduits are sized for instantaneous peak $H_2$ production, with gas blowers to maintain a slight pressure gradient. Compression and storage of one day's gas production at the field level serves to buffer diurnal fluctuation in solar radiance. Post-compression gas conduits are sized for maximum monthly average $H_2$ production. The overall facility is sized for 1 GW annual average $H_2$ production.

Although our base case assumes that $O_2$ from water splitting is vented to the atmosphere, our modeled system includes the capability to collect the $O_2$. We include this analytical capacity to enable future study of potential industrial ecology concepts involving beneficial uses for multiple co-products (including $O_2$) of energy and industrial systems. For example, $O_2$ collected from a PEC facility could be used in a high-efficiency oxy-fuel power plant integrated with $CO_2$ capture,[36] thus leveraging resources and potentially reducing system costs.

To objectively compare $H_2$ production *via* PEC processes to alternatives such as steam methane reforming, conditions for transporting the gas from the production facility to the end user should be the same. We assume the PEC facility modeled here is constructed in a remote location in the southwest US, while comparable steam methane facilities would likely be located closer to demand centers. We therefore include 300 km pipeline transport for the $H_2$ to demand location or trunk pipeline. We assume any $H_2$ distribution network (*e.g.* to end users) is the same for all $H_2$ production options, and thus is not included in the analysis.

Industrialization of the manufacture, logistics, and refurbishment of panels will be essential, as a 1 GW facility will have about 1.5 million panels under base-case conditions. The panel length and width corresponds to the inside dimensions of a standard 40-foot shipping container, to take advantage of transport by existing equipment and infrastructure. If the panel thickness is about 10 cm, 24 panels would occupy the volume of one container. Under steady-state conditions with 10% of panels replaced per year, about 17 containers would be required each day to deliver the requisite number of new panels and to take back old panels for remanufacture.

### 2.3 System components

The broader $H_2$ production facility includes the PEC cells, structural support for the cells, manifolds and pipes to conduct fluids, gas compression, storage tanks, water purification, monitoring system and roads. In a life-cycle perspective, the production, operation, and decommissioning of these components must be considered. Descriptions and assumptions of the system components are detailed below.

**2.3.1 PEC cells.** We use a membrane-separated cathode/anode geometry for the PEC cells, as our modeling informs us that this can yield good efficiency without high product crossover, which would require further purification steps. Energy requirements for producing the cells, including material sourcing and cell manufacture, is based on the LCA analysis by Zhai *et al.*[28] Production of PEC cells is modeled in three cases corresponding to low, medium ("base-case"), and high energy input. In general, more sophisticated (and energy intensive) production techniques may yield PEC cells with higher STH efficiency. We disaggregate data from Zhai *et al.*[28] to distinguish photoactive materials and production processes (photoanode, photocathode and catalysts) from all other materials and processes (membrane, encapsulation, others). Following Zhai *et al.*,[28] we further distinguish material-related energy use (including all upstream energy use for raw material extraction, primary processing and transportation) from fabrication-related energy use (including final processing of materials into functional PEC cells). Details of cell characteristics are in Table S3.†

Materials that simultaneously exhibit bandgaps suitable for efficient harvesting of solar energy, charge carrier transport properties that enable effective charge extraction, and stability under reaction environments do not currently exist. While active research is devoted to the discovery of new materials, a set of existing model materials have been selected for the present analysis. In all cases, silicon has been selected as the photocathode, whereas tungsten oxide has been selected as a model metal oxide photoanode and gallium arsenide as a model high efficiency single crystalline photoanode. We note that the band gap of tungsten oxide precludes it from obtaining the 10% efficiency of the base case and that it does not generate

 

sufficient photovoltage for direct coupling to silicon to achieve overall water splitting. However, the energy inputs for its fabrication and processing are assumed to be representative of the broad class of metal oxide semiconductors that are envisioned for use in such devices. Likewise, GaAs does not exhibit the requisite stability as a photoanode under aqueous environments and cannot be directly coupled to Si to achieve 20% STH efficiency. However, stabilization of III–V semiconductors against corrosion could enable incorporation of these materials into a solar water splitting device, and GaAs is included as a model representative of this class of III–V semiconductors, such as $Al_xGa_{1-x}As$, which may enable target efficiencies to be achieved. Optimum catalyst selection is guided by benchmarking data.[37] Similar to the case of tungsten oxide, substitution of NiMo for Co, and iridium oxide for Pt will improve efficiency without affecting the results of the device analyzed in Zhai *et al.*[28]

We assume 1 molar sulfuric acid is used as the electrolyte.¶ Based on results from Haussener *et al.*,[38] we assume that each of the two chambers containing electrolyte within the PEC cells are 1 cm thick. Multiphysics modeling finds that smaller electrolyte heights lead to unacceptable ohmic drops in the solution, whereas greater electrolyte heights yield diminishing returns. Each panel contains about 540 liters of electrolyte, and a total of 820 000 $m^3$ of electrolyte will be in service in a 1 GW facility.

**2.3.2 Panel structure.** Support and orientation for PEC cells is provided by panel structural framework. Panel integrity is provided by a perimeter frame of steel channel section (ASTM C4 × 5.4), with internal elements of steel angle section (ASTM L21/2 × 2 × 3/16) spaced at 1 m to support PEC cells. Calculations of deflection under load, described in Fig. S8,† suggest that this structural solution would be sufficiently robust. Upon this panel structural framework, PEC cells are attached, a piping manifold is installed to transport water to and gases from the PEC cells, and sensors and monitoring electronics are installed. 95% of the gross surface area of the panel is assumed to be active solar collection area, while 5% of the area is inactive due to structural or other requirements.

A simple containment vessel is installed under each panel, to collect electrolyte in case of leakage to prevent its release into the environment. We assume molded PVC plastic basins with capacity of 600 liters and wall thickness of 4 mm. We assume that PVC's susceptibility to UV degradation will be overcome in a detailed engineered system using a material with negligible impact on the net energy of the system.

Transportation of panels from factory to facility is included, assuming 300 km transport by truck. After the service life of the PEC cells (assumed to be 10 years in base case), the panels are expected to be removed from service and refurbished, with new components (PEC cells, manifold, sensors) installed in the same steel structural framework.

¶ Although we assume acidic conditions in our modeling, basic conditions (*e.g.*, 1 molar potassium hydroxide) are also possible with appropriate selection of compatible materials, and at present one set of conditions is not preferable over the other. Research is ongoing into milder pH conditions, but these are not currently viable.

**2.3.3 Piping system.** We model a hierarchical network of conduits to transport fluids (Fig. S9†). Three parallel sets of pipes are modeled to transport $H_2O$ to the PEC cells and to aggregate and transport $H_2$ (and $O_2$, when included) from the cells.

Six levels of pipe hierarchy are considered, from the smallest P5 level connecting individual PEC cells within a panel, to the largest P0 level comprising the pipelines linking the facility to a demand center (Table S4†). P5 pipes are panel manifolds, P4 and P3 pipes are within fields, P2 and P1 pipes are at the facility level, and P0 pipes link the facility to the broader system. Maximum flows through the P3, P4 and P5 levels are based on instantaneous peak production (at 1000 W $m^{-2}$ of solar radiance) of uncompressed $H_2$. After distributed compression and storage (described below) to buffer diurnal fluctuations, the maximum flows through the P0, P1 and P2 levels are based on monthly peak production (at 310 W $m^{-2}$ of solar insolation) of compressed $H_2$.

Pipe diameters at each level are based on these mass flows through the pipes, combined with heuristic recommendations of economically optimal velocities of various fluids.[39,40] Our base case assumes the use of PVC pipes, with steel pipes considered in a sensitivity analysis. Amounts of material used for pipes are based on calculated relations between flow area and specific material use for standard dimensions of North American pipes (Fig. S10†), using open-source data reporting ASTM D1785 (Poly Vinyl Chloride Plastic Pipe) and ASME B36.10 (Welded and Seamless Wrought Steel Pipe) standards.

We apply a 25% material allowance for valves and fittings, and estimate the primary energy use for pipe manufacture based on Ecoinvent[41] life-cycle inventory data for polyvinyl chloride and ASTM A106 grade carbon steel. Transport of pipes over 1000 km by train is included in the energy accounting, using mode-specific energy intensity factors for cargo transport.[42]

**2.3.4 Gas handling.** To provide a slight pressure gradient to move gases through the diffuse network from PEC cells to compressors, we assume the use of rotary lobe blowers driven by electric motors. We use one blower for every 100 panels, providing movement of 1200 liters $min^{-1}$ under conditions of maximum $H_2$ production. To remove moisture from the $H_2$ we use one refrigerated gas dryer per field (1000 panels), prior to gas compression. Electricity use data for gas blowers and dryers are based on literature from gas handling industries.[43]

We then assume compression of $H_2$ to 300 psi (2070 kPa) using one twin-stage positive displacement compressor per field. Electricity use for compression is based on Pope.[44] Pressure drop of the gas through the 300 km pipeline is estimated based on Hall,[39] and final re-compression to 300 psi for delivery is again based on Pope.[44] Embodied energy of blower and compressor hardware is based on Koornneef *et al.*,[45] assuming linear scaling with capacity.

Storage capacity is needed for PEC systems to buffer intermittent diurnal production, to achieve an on-demand functionality of $H_2$ production similar to steam methane reforming. Following Yang and Ogden,[46] we measure storage capacity as a

proportion of daily flow, and we consider one day's production storage in our base case. We assume the ideal gas law accurately governs the relation between volume and absolute pressure; the storage volume needed for 1000 panels (one field) is about 300 $m^3$ at 300 psi at a temperature of 20 °C. Storage tanks are assumed made of steel, and designed according to Peters *et al.*[47] Sensitivity parameters include the allowable metal stress, the allowance for corrosion, and the allowance for valves and fittings.

**2.3.5 Water supply.** Water is required for two purposes: feedstock for $H_2$ production, and cleaning of panel surfaces. The feedstock $H_2O$ supply for PEC $H_2$ production must be nearly pure, with very low concentrations of ions that could foul the PEC cells. Precise water purity requirements for a large-scale PEC system remain uncertain. Measured as resistivity (inversely proportional to ionic concentration), traditional electrolyzers require a purity of >1 MΩ cm at 25 °C.[48] Here we consider the use of reverse osmosis (RO) water treatment, based on energy intensity data from EERE.[49] We consider only the operating energy for water treatment, and assume the embodied energy of the RO hardware is negligible. Water vapor in $H_2$ gas is condensed and recovered with a refrigerated gas dryer. The amount of water vapor that is lost with vented $O_2$ gas is estimated based on results from the panel heating calculations (see Section 2.3.9). It is assumed that gas leaves the device at 100% relative humidity, with water losses therefore dictated by the $O_2$ gas evolution rate and the temperature of the electrolyte. On average, 6.8% of the water feedstock entering the cells is lost with the $O_2$ gas stream.

For cleaning of panels, an additional 25 liters of water per year per square meter of panel is assumed required, based on data from utility-scale PV.[50,51] A relation is expected between water use for cleaning and solar loss due to dusty panels. Studies elucidating such trade-offs are beginning to emerge (*e.g.* Mejia and Kleissl[52]), though the data are still insufficient for robust quantification. There may also be other techniques for panel cleaning such as electrostatic or air pressure methods. We therefore explore this region through sensitivity analysis of two model parameters: specific water use for panel cleaning and solar transmittance loss due to dust, glass and electrolyte.

Municipal-grade water is assumed to be transported 300 km by pipeline to the facility. Pipe details are described in Section 2.3.3. Specific energy use for water pumping is based on Plappally and Lienhard.[53] Water calculations include water that is piped to the facility and then lost as concentrate waste from the RO process; this amount is estimated at 0.39 liter for each liter of purified water used as $H_2$ feedstock. Waste management of RO concentrate is not considered in the analysis.

**2.3.6 Monitoring system.** We envision a monitoring system comprised of multiple sensors on each panel, with data transmitted to a control center *via* a wireless network. Each PEC cell has one temperature sensor, one pH sensor, and three pressure sensors (one each for $H_2$, $O_2$, and $H_2O$). At the panel level are three additional pressure sensors and two flow sensors (one each for $H_2$ and $O_2$). Measuring the low flows of $H_2O$ is not feasible at the panel level, so this is done starting at the field level, along with additional pressure sensors.

**2.3.7 Roads.** Asphalt roads accompany all P1, P2, and P3 pipes. All panels are located within 50 m of a road surface, for placement and removal with mobile cranes. The roads are 6 m wide, with a crushed stone base and bitumen asphalt wear layer to ensure adequate service life and reduce dust generation from road traffic. This accounting category also includes other ground surface interfaces, including concrete anchors for panels and concrete pads for blowers, compressors and tanks.

**2.3.8 Facility operations.** We assume a fleet of two mobile cranes and four flatbed trucks operating 12 hours per day conducting maintenance, *e.g.*, replacement of cells or panels at the end of their service life. Energy intensity data for heavy equipment is based on FAO.[54] Other maintenance of equipment and infrastructure (*e.g.*, painting) is assumed to be negligible and is not included.

**2.3.9 Panel heating.** Heating of panels may be required to prevent freezing of the electrolyte during cold weather. The freezing temperature of 1 molar sulfuric acid is approximately −5 °C. If the PEC cells drop below this temperature, they will freeze and potentially rupture, likely causing device failure. To prevent freezing, the underside of each panel may be fitted with an electrically powered strip heater to provide heating when the embedded temperature sensors determine this necessary. This heater can also be backed by a layer of insulation. We used a computational model to assess the degree of heating required for the panels, to estimate its effect on the facility's net energy production. Given the small aspect ratio of the modules (thickness divided by length or width), a 1-D finite-difference transient heat transfer model was constructed, with coupled heat transfer equations solved for each hour of the year for the top window, anolyte, light absorber assembly, catholyte, case backing, strip heater and (when applicable) insulation layers. It was assumed that the panels only transfer heat out to the environment *via* radiation and convection. These modules would heat up in the daytime due to the conversion of insolation into waste heat in the light absorber assembly and in the semitransparent top window; joule heating of the electrolyte was ignored given the low current densities of this device. If the temperature of the device dropped below a temperature threshold of −2.5 °C, a 1-D steady-state heat transfer model was used to estimate the required heater energy input to prevent the electrolyte temperature from dropping further. This minimum temperature threshold is greater than the electrolyte freezing temperature to provide an operational safety margin.

In this model, historical, measured typical meteorological year data from NREL[55] was used to simulate the hourly ambient weather conditions that the panels would experience. The position of the sun with respect to the panel was then calculated, and derating factors from Notton[56] were used to calculate the total combined beam and diffuse radiative solar resource reaching the panel. Empirical formulae were used to estimate the effective temperature of the sky to which the panels radiated in clear conditions[57] and cloudy conditions.[58] Additional empirical formulae were used to calculate the wind-induced forced convective heat transfer coefficients;[59] natural convective heat transfer coefficients;[60–63] and the internal convective heat

 

transfer coefficients in the anolyte and catholyte.[60] These insolation values and heat transfer coefficients were recalculated for each hour of the year based upon ambient conditions, device temperatures and device orientation. The thermal material properties of the cell components were sourced from Notton *et al.*[56] and Incropera.[60] Thermal properties of electrolyte and ambient air are temperature-dependent, whereas the other components of the module are constant and assumed to have properties corresponding to 27 °C.

The estimated total annual electricity requirement for heating varies by location, with Daggett requiring the most at 11.0 kW h per $m^2$ per year, and Phoenix needing the least at 0.6 kW h $m^{-2}$ $yr^{-1}$. More details are in Table S5.†

**2.3.10 Decommissioning.** At some point in the future, the facility will reach the end of its service life and will be decommissioned. This entails removing or remediating the infrastructure and equipment comprising the facility, and its safe disposal or recycling. Following the method used in the series of energy system life cycle assessments summarized by NETL,[64] we assume that decommissioning requires 10% of the energy used for initial construction of the facility BOS.

## 3. Results

Fig. 2 shows the annual energy balance of the $H_2$ production facility in operation, under base-case conditions at 10% STH efficiency. The energy content of the $H_2$ produced corresponds to 31.5 PJ of primary energy per year, which is equivalent to 1 GW continuous power for one year. From this positive value is subtracted the primary energy needed to operate the production system. The largest single energy use is for panel replacement, which uses 8.7 PJ per year under steady-state conditions with a 10 year panel life span (*i.e.* 10% of all panels in the facility are replaced each year). Gas compression is the second largest energy input (4.9 PJ per year), 67% of which is for initial compression and 33% is for re-compression after pipeline transport. Panel heating to avoid electrolyte freezing requires a less significant energy input (1.5 PJ per year). Together with other energy inputs of 0.8 PJ per year, the net energy delivered is 15.7 PJ of primary energy per year, under base-case conditions.

Fig. 3 shows the initial energy inputs required to construct the 1 GW $H_2$ facility; for the base-case conditions, construction will need 124 PJ of primary energy. The estimated energy input for decommissioning of the facility at the end of its service life is 4 PJ. These one-time inputs are compared to the annual delivered energy of the facility (from Fig. 2), shown as a dashed line. Under base case conditions, it will take about 8.1 years of operation to deliver energy that is equivalent to that used for initial construction and final decommissioning. Over the 40 year projected service life of the facility, the EROEI is 1.7 and the life-cycle primary energy balance is +500 PJ.

Fig. 4 shows the change in three net energy metrics (life-cycle energy balance, EROEI, energy payback time) due to variation of individual parameters between low and high estimates. The 15 parameters that most significantly affect each metric are shown. STH efficiency is the parameter variation causing the most significant change in all three metrics. Other significant parameters include PEC cell life span, BOS life span, photo-active cell fabrication energy use, and non-photo-active cell material energy use.

The three parameters of STH efficiency, PEC cell life span and facility life span show prominently on the sensitivity diagrams in Fig. 4. We explore the relations between these three parameters in more detail in Table 1. While most parameter combinations (including the base-case) show net positive life-

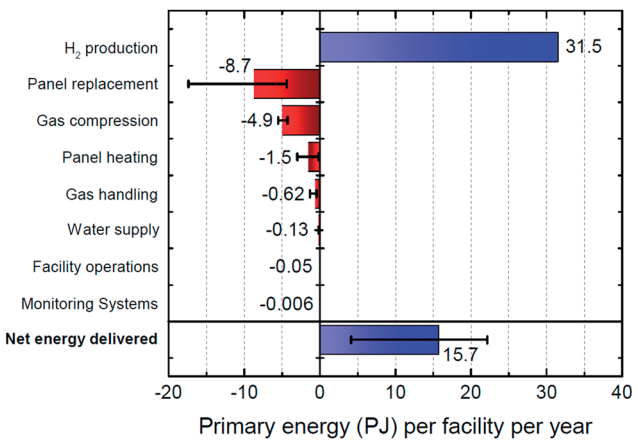


Fig. 2 Annual energy balance of 1 GW (continuous annual average) $H_2$ production facility in operation (PJ per year). Energy use for panel replacement is based on steady-state conditions with 10 year life span (10% of panels replaced each year) and base-case energy use for cell materials and fabrication. Error bars for "Panel replacement" show 5- and 20 year life spans. Error bars for "Panel heating" are based on coldest and warmest geographic locations. Error bars for other categories are based on Monte Carlo simulation.

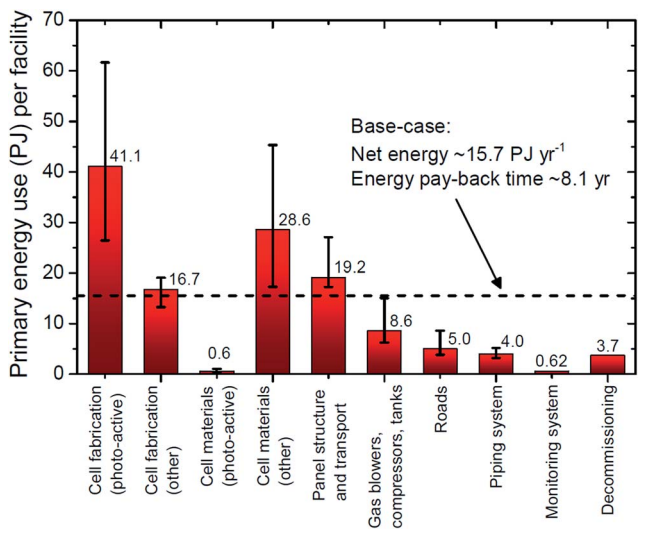


Fig. 3 One-time primary energy inputs (PJ) required to construct and decommission a 1 GW (continuous annual average) facility. The base-case annual delivered energy of the completed facility is shown as a dashed line. Error bars for cell fabrication and cell materials correspond to low and high cases of Zhai *et al.*[28] Error bars on other energy inputs are based on Monte Carlo simulation.

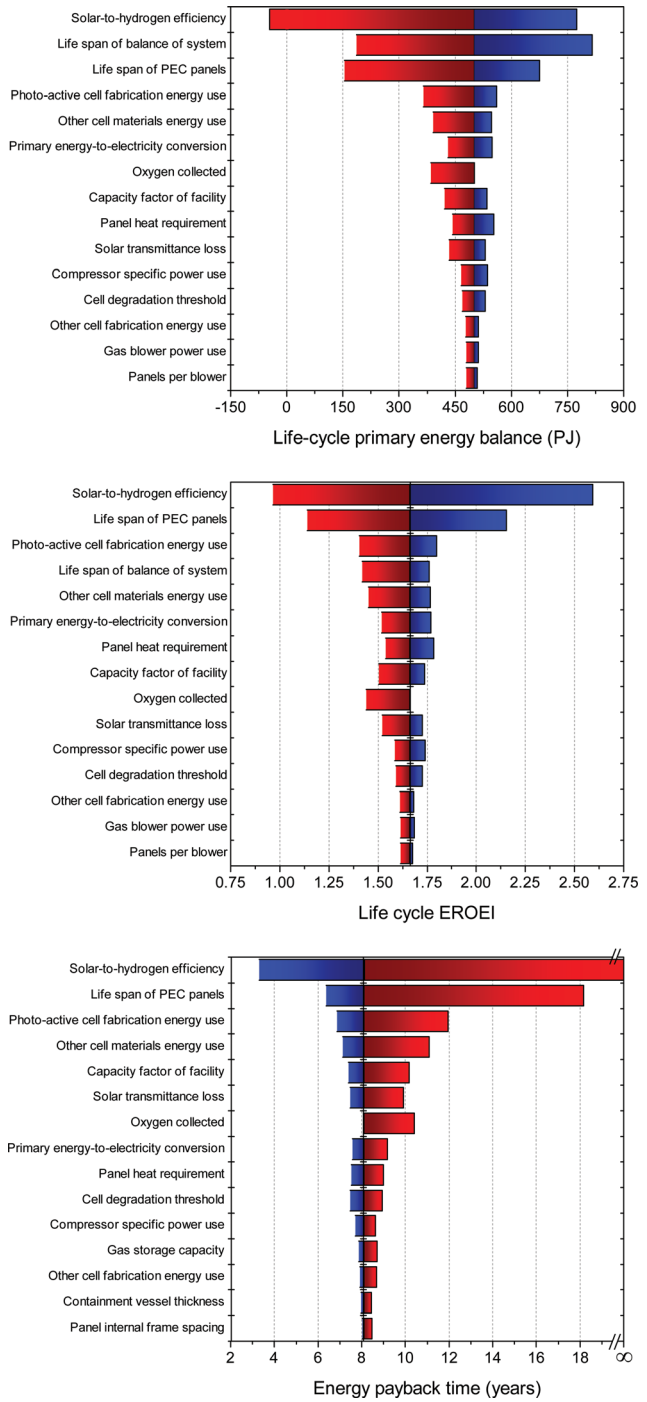


Fig. 4 Change in base-case life-cycle energy balance, EROEI and energy payback time due to variation of individual parameters between low and high estimates. Specific values for low-, base-, and high-cases are given in Table S1.†

cycle energy balance (and thus life-cycle EROEI greater than one) and energy payback times of less than 10 years, some combinations result in net negative life-cycle energy balance, particularly when the STH efficiency is 5% and the panel life span is 5 years. With 20% STH efficiency, EROEI is in the range of 2 to 3, and energy payback time is about 3 to 4 years.

One may expect that more sophisticated (and energy intensive) production techniques may yield PEC cells with higher STH efficiency. Table 2 shows the modeled net energy metrics as a function of STH efficiency and energy input for photo-active materials and fabrication. At high photo-active energy input and 5% STH efficiency we again see net negative life-cycle energy balance and life-cycle EROEI less than one.

Required land area and solar collection area are listed in Table 3, and are significantly and directly affected by changes in STH efficiency. With the base-case 10% STH efficiency, a facility will have about 41 $km^2$ of PEC surface area. The facility as a whole will occupy about 180 $km^2$, if it is in the contiguous format that is modeled here (Fig. S5†). This corresponds to about 2.1 hectares of land used per MW h per year of primary energy. This compares to a generation-weighted average land use of 2.3 ha MW per h per year for large-scale fixed-panel PV facilities in the US,[65] after conversion from electricity to primary energy units using the method described in Section 2.1. Depending on topography and other factors, it may be necessary to arrange the facility in other non-contiguous formats which would increase the total land area occupied by the facility. Ong *et al.*[65] reported that the average total land area of large-scale fixed-panel PV facilities in the US is about 30% greater than the land area directly occupied by the solar arrays, access roads, substations, service buildings and other infrastructure.

The land area for the facility is affected by the packing factor of the panels, defined as the ratio of panel area to land area. The packing factor in this analysis is 0.23, which is lower than the average packing factor of 0.47 for fixed-panel PV arrays in the US.[65] Packing factor is largely determined by spacing between rows of panels, which also determines losses due to shading by adjacent panels when the sun is low in the sky. Our inter-row spacing, and hence packing factor, is based on the 10° shading angle used by James *et al.*[26] and Pinaud *et al.*[27] If the shading angle is increased to 20°, the packing factor increases to 0.39 and the land area required with 10% STH efficiency decreases to 107 $km^2$. With a 30% shading angle, the packing factor increases to 0.51 and the land area decreases to 81 $km^2$. These calculations are based simply on geometry, however, and do not consider the $H_2$ production losses that would occur due to increased inter-panel shading.

A 1 GW $H_2$ facility will need an average of 5800 tons of treated feedstock water per day, of which about 370 tons will be lost as water vapor with vented $O_2$ and the remainder will be split into $H_2$ and $O_2$. For cleaning panels, an additional 2800 tons per day of water is required under base-case conditions. An additional 2200 tons per day of water will be contained in RO concentrate, a byproduct of the water purification process. The total water use of the facility is 10 900 tons per day, or about 4 million cubic meters per year. For comparison, Lake Mead, the reservoir created above the Hoover dam in the southwest US, has a capacity of about 34 000 million cubic meters of water.

An average of 4800 tons per day of $O_2$ is produced during water splitting in the 1 GW facility, which in the base-case is vented into the air. To collect and use the $O_2$, production and operation of a parallel pipe network and gas handling system is required. The facility net energy metrics are slightly affected by this additional energy use. The life-cycle net energy balance

 

Table 1 Life cycle net energy metrics for a 1 GW (continuous annual average) $H_2$ production facility, under various assumptions of facility life span, cell life span, and STH efficiency. The numbers in bold represent base-case conditions. N/A means "not applicable"

| Facility life span | 20 years | | | 40 years | | | 60 years | | |
|---|---|---|---|---|---|---|---|---|---|
| PEC cell life span | 5 years | 10 years | 20 years | 5 years | 10 years | 20 years | 5 years | 10 years | 20 years |
| **5% STH** | | | | | | | | | |
| Energy inputs (PJ) | 1123 | 775 | 602 | 2002 | 1307 | 959 | 2881 | 1838 | 1317 |
| Energy outputs (PJ) | 631 | 631 | 631 | 1261 | 1261 | 1261 | 1892 | 1892 | 1892 |
| Life-cycle energy balance (PJ) | −492 | −145 | 29 | −740 | −45 | 302 | −989 | 54 | 575 |
| Life-cycle EROEI | 0.56 | 0.81 | 1.05 | 0.63 | 0.97 | 1.31 | 0.66 | 1.03 | 1.44 |
| Energy payback time (years) | N/A | N/A | 17.9 | N/A | N/A | 17.9 | N/A | 49.1 | 17.9 |
| **10% STH** | | | | | | | | | |
| Energy inputs (PJ) | 618 | 444 | 357 | 1107 | **760** | 586 | 1597 | 1076 | 815 |
| Energy outputs (PJ) | 631 | 631 | 631 | 1261 | **1261** | 1261 | 1892 | 1892 | 1892 |
| Life-cycle energy balance (PJ) | 13 | 187 | 274 | 154 | **502** | 675 | 295 | 816 | 1077 |
| Life-cycle EROEI | 1.02 | 1.42 | 1.77 | 1.14 | **1.66** | 2.15 | 1.18 | 1.76 | 2.32 |
| Energy payback time (years) | 18.2 | 8.1 | 6.4 | 18.2 | **8.1** | 6.4 | 18.2 | 8.1 | 6.4 |
| **20% STH** | | | | | | | | | |
| Energy inputs (PJ) | 365 | 278 | 235 | 660 | 486 | 399 | 955 | 694 | 564 |
| Energy outputs (PJ) | 631 | 631 | 631 | 1261 | 1261 | 1261 | 1892 | 1892 | 1892 |
| Life-cycle energy balance (PJ) | 266 | 353 | 396 | 601 | 775 | 862 | 937 | 1198 | 1328 |
| Life-cycle EROEI | 1.73 | 2.27 | 2.69 | 1.91 | 2.59 | 3.16 | 1.98 | 2.72 | 3.35 |
| Energy payback time (years) | 4.2 | 3.3 | 3.0 | 4.2 | 3.3 | 3.0 | 4.2 | 3.3 | 3.0 |

Table 2 Life cycle net energy metrics for a 1 GW (continuous annual average) $H_2$ production facility, under various assumptions of STH efficiency and energy inputs for photo-active cell materials and fabrication. The numbers in bold represent base-case conditions

| STH efficiency | 5% | 10% | 20% |
|---|---|---|---|
| **Low energy intensity of photo-active materials and fabrication** | | | |
| Life-cycle energy balance | 76 | 562 | 805 |
| Life-cycle EROEI | 1.06 | 1.80 | 2.77 |
| Energy payback time | 29.7 | 6.8 | 2.9 |
| **Medium energy intensity of photo-active materials and fabrication** | | | |
| Life-cycle energy balance | −45 | **502** | 775 |
| Life-cycle EROEI | 0.97 | **1.66** | 2.59 |
| Energy payback time | N/A | **8.1** | 3.3 |
| **High energy intensity of photo-active materials and fabrication** | | | |
| Life-cycle energy balance | −323 | 362 | 706 |
| Life-cycle EROEI | 0.80 | 1.40 | 2.27 |
| Energy payback time | N/A | 12.0 | 4.3 |

Table 3 PEC solar collection area and gross facility land area ($km^2$) required for STH efficiencies of 5%, 10% and 20%

| | | 5% STH | 10% STH | 20% STH |
|---|---|---|---|---|
| PEC solar collection area | $km^2$ | 82.2 | 41.1 | 20.6 |
| Gross facility land area | $km^2$ | 361 | 180 | 90 |

decreases by 116 PJ to +385 PJ. EROEI decreases to 1.4. The energy payback time increases to 10.4 years. Per ton of $O_2$ that is collected, compressed and delivered, 1.7 GJ of additional energy is used. This is less than a fifth of the reported energy intensity of conventional $O_2$ production technologies,[41] suggesting there may be advantages to capturing the $O_2$ and coupling it with an $O_2$-consuming facility such as an oxy-fuel combustion electricity plant.

The material used for the piping system has a modest effect on net energy metrics. The base-case assumes the use of PVC pipes. If steel pipes are used instead, the life cycle primary energy balance drops from 502 PJ to 496 PJ. The EROEI drops from 1.66 to 1.65, and the energy payback time increases from 8.1 years to 8.5 years. Primary energy use for manufacture and transport of PVC and steel pipes for $H_2$, $O_2$ and $H_2O$ at the P0 through P5 levels is shown in Fig. S11.†

# 4. Discussion

To provide usable energy to society, a renewable energy technology must harness and deliver more energy than is needed to produce and operate the technology, resulting in positive net energy. This prospective net energy analysis shows that PEC $H_2$ production technologies have the potential to deliver significant amounts of net energy. The most important variables include the STH efficiency, the life span of the PEC cells, the energy intensity of fabricating the photo-active components of the cells, and the life span of the BOS of the facility.

Achieving a high STH efficiency while retaining a long device lifetime remains a primary challenge within the solar fuels research field. The factors contributing to STH efficiency of an integrated PEC system can be grouped into five general categories: (1) efficiency of light absorption, (2) efficiency of charge separation and extraction, (3) efficiency of catalysis, (4) effectiveness of product separation and (5) efficiency losses due to series resistance. While series resistance losses can be

mitigated by appropriate device architecture and electrolyte selection, the first three factors rely on development of precisely tailored materials and material assemblies. Light absorption is accomplished in semiconductor materials, often in stacked tandem configurations, and maximum theoretical STH efficiencies are defined by the bandgaps of these materials.[66] However, approaching the theoretical STH efficiency limit requires that photo-generated charge carriers can be extracted. Therefore, the diffusion length of these carriers, which is defined by fundamental material limits, as well as crystal quality, must be well matched to the optical absorption depth in the material. The total photovoltage that must be supplied by the semiconductor light absorbers is equal to the thermodynamic potential for water splitting, 1.23 V, plus the additional potential required for catalyzing the reaction at a given current density, typically a total of ~0.4 V. In general, increased photovoltage comes at the cost of photocurrent density, which is akin to efficiency. Consequently, the semiconductors must be coupled to catalysts that can drive the oxygen evolution reaction (OER) and hydrogen evolution reaction (HER) with minimal overpotential requirements. While HER catalysts that operate with very low overpotentials are available, OER catalysts require >0.3 V overpotential and very few are stable under acidic conditions.[37] Discovery of new OER catalysts with reduced overpotentials and an expanded pH stability window is an important avenue for increasing ultimate efficiency of integrated PEC devices. In addition, product separation is a critical factor influencing the overall efficiency of the device. Without effective product separation, significant cross-over or co-evolution of $H_2$ and $O_2$ would lead to recombination and formation of an explosive mixture over large areas. Creating innovative methods for separating product gases that are both efficient and cost effective will be a key factor that determines overall efficiency of the technology.

While a variety of semiconductor materials are available for harvesting solar energy with high efficiency, the great majority of these materials are not stable against (photo) corrosion under the conditions required for solar water splitting. As shown in the present life-cycle energy assessment, the life span of the PEC cells significantly affects the net energy delivered by the facility, due to the energy intensity of cell production. As cell life spans decrease, more energy must be invested in cell production for a given fuel output. Intensive research efforts are underway to discover new semiconductor materials that provide suitable band gaps, photocarrier transport properties, and long term stability under both operational (illuminated daytime) and stand-by (dark nighttime) conditions. However, no materials matching these requirements are presently available. An alternate approach is based on the application of thin film corrosion protection layers that enable charge transport from semiconductors to catalysts but impart stability to otherwise unstable materials.[67–69] Recent advancements provide some promise, but thin film corrosion protection over many years of service represents a significant technical challenge.

Similar to PV manufacturing,[70] the largest single use of energy is for the fabrication of photo-active cell components including photoanodes, photocathodes and catalysts. For solar PV manufacturing, the key drivers for reducing cost and energy intensity per cell are scale of the manufacturing facility, supply chain advantages, and innovation.[71] Given the diversity of the materials and processes involved, there is no single strategy for reducing overall energy inputs. Materials that can be extracted, recycled, or recovered with low energy inputs are desired, and thermal budgets associated with manufacture and processing should be minimized. For example, the high melting point of silicon and the requirement that bulk single crystals be processed from melt ($T_{melt} = 1414\ ^{\circ}C$) results in a significant energy burden that has driven research into thin film materials. Nevertheless, higher efficiencies devices are generally obtained from high quality single crystalline materials compared to devices made from less energy-intensive thin film materials. As a result, single crystalline silicon PV cells remain competitive with the range of thin film PV systems currently available. For PEC water splitting, significant emphasis is placed on earth abundant metal oxide materials that exhibit improved stability over non-oxide semiconductors and require much lower processing temperatures (*i.e.* energy inputs). However, these materials typically exhibit bandgaps that are too wide for effective utilization of the solar spectrum and poor carrier transport properties that preclude ultimate efficiencies from being approached. The present work points to a primary need for developing materials that exhibit high efficiency and long lifetime, though an important secondary goal should be the extension to materials that require low energy budgets for fabrication. An important metric for assessing the competiveness of these technologies will be their cost to performance ratio. Other factors that may improve efficiency and reduce the energy input for processing the absorber and catalysis assembly include: reducing the amount of material required for each (optimizing the device), decreasing the amount of material loss during fabrication, developing innovative processes for creating materials with reduced energy consumption, reducing purification requirements of materials while still maintaining performance, and recycling and reusing materials.[70] The module fabrication for the cell, which includes the supporting structures for the light absorber, window and connectors for the cell, may also be a significantly energy sink if these components are not low cost, reusable and/or recyclable.

Another significant energy input is for compressing the $H_2$ that is produced by the facility. Conventional positive-displacement gas compressors are assumed to be used for compression. Another option exists for compression to take place at the PEC cell level, using an overpotential of 0.06 eV per atm to drive $H_2$ production at elevated pressure.[72] While we did not model this possibility, we acknowledge it as an area of future exploration. This would require maintaining cells and panels above atmospheric pressure, which would involve trade-offs between the decreased energy requirements for gas compression and the higher performance needs of the cell encapsulation materials. This approach may be feasible if solar concentration were to be implemented, but would otherwise make the cell design significantly more complex.

Analyzing the effective future role of an emerging energy technology is challenging due to the dynamic nature of energy

 

systems, which include supply and demand technologies that evolve and expand over time. PEC technologies may compete against alternative $H_2$ production methods including from natural gas with $CO_2$ capture and sequestration (CCS), coal with CCS, and electrolysis using renewable electricity sources. The facility modeled here is a very large unit intended for utility-scale production of $H_2$. It produces an annual average of 6.8 million $Nm^3$ of $H_2$ per day, considerably larger than the 1.5 million $Nm^3$ per day scale that is typical of current major oil refineries.[73] However, it is comparable in energy output to large natural gas-, coal-fired or nuclear power plants, with typical sizes of 300–2000 MW electrical output, and primary energy inputs roughly three times these values. Important work remains to determine whether this scale of production is optimal, and to identify relevant scaling factors for PEC facilities of varying size.

The amount of $H_2$ required to power all the light-duty vehicles in the US is approximately 5000 PJ per year today, or the output of roughly 160 of the 1 GW facilities modeled here (see ESI† for details). As the fuel efficiency of hydrogen vehicles is anticipated to increase in future years, the number of facilities required would fall to ~130 by 2050, even though the number of vehicle-kilometers travelled would have increased ~40% under base case assumptions. The number of facilities required to power the light-duty vehicle fleet would account for approximately 50% of US hydrogen demand, assumed to total 60 Mt $H_2$ per year in our 2050 scenario. With cost-competitive $H_2$ production and widespread demand as a vehicle fuel, it is likely that utilization would expand to other parts of the transportation system (especially trucks and buses) as well as industrial heating and some electricity generation.

Electricity inputs for facility operation have been assumed here to be grid electricity. Alternately, land adjacent to the PEC facility could be used to produce PV electricity. This solution would elegantly match the varying rate of $H_2$ produced by PEC panels to the rate of PV electricity produced and used for gas handling and compression. Assuming PV panels with 15% solar-to-electricity conversion efficiency, roughly 2.7 $km^2$ of PV collection area will be needed to produce the electricity used for operation of the facility. Further assuming the same ratio of land area to panel area as the PEC panels, about 12 $km^2$ of land will be needed for the PV panels, an additional 7% to the total land area required. This estimate does not consider possible mismatch between power generation characteristics of the PV panels and the load of the facility equipment. However, since almost all electricity would be used during $H_2$ production periods (*e.g.*, daytime), any mismatch would likely be small.

Our modeling suggests that in warm climates, the heating energy input needed to avoid freezing of electrolyte is a relatively small portion of the operating energy budget. However, in cold locations, heating energy can be a significant portion of the total energy production, and thus installation of facilities there may not be advisable. For instance, Albuquerque, NM has a solar resource comparable to that of the other locations analyzed here, but between 27% and 58% of the energy produced at the site would be required for heating during a typical year, given the same variation of parameters listed in Table S5.† In order to reduce overall heating energy input, one should first reduce the minimum safe operating temperature as much as possible. For example, if substances that do not harm the operation of the device can be introduced to the electrolyte, the freezing temperature of the electrolyte may be reduced, thus reducing the required heating energy input. Following that, installing a low-emissivity coating on the window material is helpful to reduce heating energy input. Installing insulation around the heating element may also be useful in colder climates, but this will increase energy input in warm climates because "free" heating of the device at near-freezing ambient conditions to offset low effective radiative sky temperatures is prevented by the insulation. Incorporating some means of preventing the panels from freezing during abnormally cold weather is advisable in all locations, given the necessity of ensuring device longevity to enhance the facility's net energy balance.

This modeling exercise is the first effort that we are aware of to estimate the net energy of large-scale PEC $H_2$ production. Previous net energy analyses have, however, been conducted on other energy technologies. Fossil fuels typically have relatively high net energy, because these fuels are concentrated stores of energy that require comparatively little energy inputs to access and exploit. For example, the EROEI of global petroleum production is about 17, while that of US petroleum production is about 11.[74] These values are declining over time, as more accessible oil deposits are depleted and more remote deposits are exploited; the EROEI of oil sands and ultra-deep-water oil production is less than 10. Technologies for harnessing renewable energies typically have lower net energy performance, because renewable energy is often more diffuse than fossil fuels, thus more extensive infrastructure is needed to capture and deliver a unit of usable energy. Another important distinction is whether the delivered energy is in the form of electricity or a storable fuel. This affects both how the energy can be used by society, as well as methodological issues in comparing primary and derived energy sources (as discussed in Section 2.1). Electricity production from PV has an EROEI of about 6, with a range from 3 to 10.[75] The net energy of ethanol, a renewable and storable fuel, is the subject of considerable debate. For example, Pimentel[76] asserted that corn-based ethanol has an EROEI less than one, such that producing it consumes more energy than it contains. Oliveira *et al.*,[77] on the other hand, estimated the EROEI of US corn-based ethanol to range from 1.03 to 1.12, and that of Brazilian sugarcane-based ethanol to range from 3.1 to 3.9.

# 5. Conclusions

Large-scale harnessing and use of renewable energy sources will be increasingly important in the future, to ensure sustainable energy resources and reduce climate impacts. Creating storable fuels from solar energy is a way to overcome the inherent intermittency of solar radiation. Due to the diffuse nature of solar energy flows, considerable infrastructure is needed to capture large quantities of solar energy. Hydrogen production

using PEC water splitting is one promising approach to harness solar energy and convert it directly to a storable fuel.

We have conducted a preliminary engineering design of a hypothetical large-scale PEC $H_2$ production facility with an energy output equivalent to 1 GW continuous annual average. We find that under base-case conditions the energy payback time is 8.1 years, the energy return on energy invested (EROEI) is 1.7 and the life-cycle primary energy balance over the projected service life of the facility is +500 PJ. The most important system parameters affecting the net energy are the STH conversion efficiency and the service life of the PEC cells. With STH efficiency of 20% and PEC cell life span of 20 years, an energy payback time of around 3 years, and EROEI of around 3, may be obtained. Other important parameters include the service life of the facility, and the energy intensity of cell materials and fabrication. Parameters associated with the BOS of the facility, including construction and operation of the liquid and gas handling infrastructure, play a smaller role.

Although this analysis is being performed at an early stage of PEC technology development, and involves many assumptions, it provides key insights to the most impactful avenues for research in the area of solar fuels generation. Many research needs have been identified by groups working in this field, all of which require significant focus but may not, in the end, lead to technological improvements. Through this assessment we have identified priority topics for further research, as these factors will be essential determinates of the energetic effectiveness of eventual large-scale PEC solar energy technology.

## Acknowledgements

This material is based upon work performed by the Joint Center for Artificial Photosynthesis, a DOE Energy Innovation Hub, supported through the Office of Science of the US Department of Energy under Award Number DE-SC0004993.

## References

1 S. Chu and A. Majumdar, Opportunities and challenges for a sustainable energy future, *Nature*, 2012, **488**, 294.
2 M. A. Green, K. Emery, Y. Hishikawa, W. Warta and E. D. Dunlop, Solar cell efficiency tables (version 43), *Progress in Photovoltaics: Research and Applications*, 2014, vol. 22, p. 1.
3 P. Denholm and G. L. Kulcinski, Life cycle energy requirements and greenhouse gas emissions from large scale energy storage systems, *Energy Convers. Manage.*, 2004, **45**, 2153.
4 R. E. Blankenship, D. M. Tiede, J. Barber, G. W. Brudvig, G. Fleming, M. Ghirardi, M. R. Gunner, W. Junge, D. M. Kramer, A. Melis, T. A. Moore, C. C. Moser, D. G. Nocera, A. J. Nozik, D. R. Ort, W. W. Parson, R. C. Prince and R. T. Sayre, Comparing photosynthetic and photovoltaic efficiencies and recognizing the potential for improvement, *Science*, 2011, **332**, 805.
5 H. von Blottnitz and M. A. Curran, A review of assessments conducted on bio-ethanol as a transportation fuel from a net energy, greenhouse gas, and environmental life cycle perspective, *J. Cleaner Prod.*, 2007, **15**, 607.
6 N. S. Lewis and D. G. Nocera, Powering the planet: Chemical challenges in solar energy utilization, *Proc. Natl. Acad. Sci. U. S. A.*, 2006, **103**, 15729.
7 B. Kumar, M. Llorente, J. Froehlich, T. Dang, A. Sathrum and C. P. Kubiak, Photochemical and photoelectrochemical reduction of $CO_2$, *Annu. Rev. Phys. Chem.*, 2012, **63**, 541.
8 M. G. Walter, E. L. Warren, J. R. McKone, S. W. Boettcher, Q. Mi, E. A. Santori and N. S. Lewis, Solar water splitting cells, *Chem. Rev.*, 2010, **110**, 6446.
9 R. E. Rocheleau, E. L. Miller and A. Misra, High-efficiency photoelectrochemical hydrogen production using multijunction amorphous silicon photoelectrodes, *Energy Fuels*, 1998, **12**, 3.
10 O. Khaselev, A. Bansal and J. Turner, High-efficiency integrated multijunction photovoltaic/electrolysis systems for hydrogen production, *Int. J. Hydrogen Energy*, 2001, **26**, 127.
11 N. A. Kelly and T. L. Gibson, Design and characterization of a robust photoelectrochemical device to generate hydrogen using solar water splitting, *Int. J. Hydrogen Energy*, 2006, **31**, 1658.
12 S. Licht, B. Wang, S. Mukerji, T. Soga, M. Umeno and H. Tributsch, Efficient solar water splitting, exemplified by $RuO_2$-catalyzed AlGaAs/Si photoelectrolysis, *J. Phys. Chem. B*, 2000, **104**, 8920.
13 G. Peharz, F. Dimroth and U. Wittstadt, Solar hydrogen production by water splitting with a conversion efficiency of 18%, *Int. J. Hydrogen Energy*, 2007, **32**, 3248.
14 K. Fujii, S. Nakamura, M. Sugiyama, K. Watanabe, B. Bagheri and Y. Nakano, Characteristics of hydrogen generation from water splitting by polymer electrolyte electrochemical cell directly connected with concentrated photovoltaic cell, *Int. J. Hydrogen Energy*, 2013, **38**(34), 14424.
15 T. J. Jacobsson, V. Fjallstrom, M. Sahlberg, M. Edoff and T. Edvinsson, A monolithic device for solar water splitting based on series interconnected thin film absorbers reaching over 10% solar-to-hydrogen efficiency, *Energy Environ. Sci.*, 2013, **6**, 3676.
16 S. Y. Reece, J. A. Hamel, K. Sung, T. D. Jarvi, A. J. Esswein, J. J. H. Pijpers and D. G. Nocera, Wireless solar water splitting using silicon-based semiconductors and earth-abundant catalysts, *Science*, 2011, **334**, 645.
17 J. Brillet, J.-H. Yum, M. Cornuz, T. Hisatomi, R. Solarska, J. Augustynski, M. Graetzel and K. Sivula, Highly efficient water splitting by a dual-absorber tandem cell, *Nat. Photonics*, 2012, **6**, 824.
18 F. F. Abdi, L. Han, A. H. M. Smets, M. Zeman, B. Dam and R. van de Krol, Efficient solar water splitting by enhanced charge separation in a bismuth vanadate-silicon tandem photoelectrode, *Nat. Commun.*, 2013, **4**, 2195.
19 M. R. Shaner, K. T. Fountaine, S. Ardo, R. H. Coridan, H. A. Atwater and N. S. Lewis, Photoelectrochemistry of core–shell tandem junction n–p+-Si/n-$WO_3$ microwire array photoelectrodes, *Energy Environ. Sci.*, 2014, **7**, 779.

 

20 C. Liu, J. Tang, H. M. Chen, B. Liu and P. Yang, A fully integrated nanosystem of semiconductor nanowires for direct solar water splitting, *Nano Lett.*, 2013, **13**, 2989.
21 J. A. Turner, Sustainable hydrogen production, *Science*, 2004, **305**, 972.
22 C. Graves, S. D. Ebbesen, M. Mogensen and K. S. Lackner, Sustainable hydrocarbon fuels by recycling $CO_2$ and $H_2O$ with renewable or nuclear energy, *Renewable Sustainable Energy Rev.*, 2011, **15**, 1.
23 NHA (National Hydrogen Association), *Hydrogen and Fuel Cells: The US Market Report*, 2010, web-accessed at http://www.hydrogenassociation.org/.
24 EC (European Commission), *World Energy Technology Outlook*, 2006, web-accessed at http://ec.europa.eu/research/energy/pdf/weto-h2_en.pdf.
25 EIA (Energy Information Administration), *International Energy Outlook*, 2013, web-accessed at http://www.eia.gov/forecasts/ieo/.
26 B. D. James, G. N. Baum, J. Perez and K. N. Baum, *Technoeconomic Analysis of Photoelectrochemical (PEC) Hydrogen Production, Final Report, Direct Technologies, DOE Contract Number GS-10F-009J*, 2009.
27 B. A. Pinaud, J. D. Benck, L. C. Seitz, A. J. Forman, Z. Chen, T. G. Deutsch, B. D. James, K. N. Baum, G. N. Baum, S. Ardo, H. Wang, E. Miller and T. F. Jaramillo, Technical and economic feasibility of centralized facilities for solar hydrogen production *via* photocatalysis and photoelectrochemistry, *Energy Environ. Sci.*, 2013, **6**, 1983.
28 P. Zhai, S. Haussener, J. Ager, R. Sathre, K. Walczak, J. Greenblatt and T. McKone, Net primary energy balance of a solar-driven photo-electrochemical water-splitting device, *Energy Environ. Sci.*, 2013, **6**, 2380.
29 M. Spielmann, R. W. Scholz, O. Tietje and P. de Haan, Scenario modelling in prospective LCA of transportation systems: Application of formative scenario analysis, *Int. J. Life Cycle Assess.*, 2005, **10**(5), 325.
30 K. Coughlin, *Projections of Full-fuel-cycle Energy and Emission Metrics, Report LBNL-6025E, Lawrence Berkeley National Laboratory*, 2013.
31 M. Raugei, P. Fullana-i-Palmer and V. Fthenakis, The energy return on energy investment (EROI) of photovoltaics: Methodology and comparisons with fossil fuel lifecycles, *Energy Policy*, 2012, **45**, 576.
32 EERE (US DOE Energy Efficiency and Renewable Energy), Comparison of Fuel Cell Technologies, 2011, web accessed at http://www1.eere.energy.gov/hydrogenandfuelcells/fuelcells/pdfs/fc_comparison_chart.pdf.
33 Z. Chen, T. F. Jaramillo, T. G. Deutsch, A. Kleiman-Shwarsctein, A. J. Forman, N. Gaillard, R. Garland, K. Takanabe, C. Heske, M. Sunkara, E. W. McFarland, K. Domen, E. L. Miller, J. A. Turner and H. N. Dinh, Accelerating materials development for photoelectrochemical (PEC) hydrogen production: Standards for methods, definitions, and reporting protocols, *J. Mater. Res.*, 2010, **25**, 3.
34 S. Haussener, S. Hu, C. Xiang, A. Z. Weber and N. S. Lewis, Simulations of the irradiation and temperature dependence of the efficiency of tandem photoelectrochemical water-splitting systems, *Energy Environ. Sci.*, 2013, **6**, 3605.
35 NREL (National Renewable Energy Laboratory), *PV-Watts: A performance calculator for grid-connected PV systems*, 2013, web-accessed at http://rredc.nrel.gov/solar/calculators/pvwatts/version1/.
36 G. Scheffknecht, L. Al-Makhadmeh, U. Schnell and J. Maier, Oxy-fuel coal combustion: A review of the current state-of-the-art, *Int. J. Greenhouse Gas Control*, 2011, **5**(S1), S16.
37 C. C. L. McCrory, S. H. Jung, J. C. Peters and T. F. Jaramillo, Benchmarking heterogeneous electrocatalysts for the oxygen evolution reaction, *J. Am. Chem. Soc.*, 2013, **135**, 16977.
38 S. Haussener, C. Xiang, J. Spurgeon, S. Ardo, N. S. Lewis and A. Z. Weber, Modeling, simulation, and design criteria for photoelectrochemical water-splitting systems, *Energy Environ. Sci.*, 2012, **5**, 9922.
39 S. Hall, *Rules of Thumb for Chemical Engineers*, Elsevier, 2012.
40 D. R. Woods, *Rules of Thumb in Engineering Practice*, Wiley-VCH, Weinheim, 2007.
41 Ecoinvent, *Ecoinvent v2.2 Life Cycle Inventory (LCI) database*, 2012, http://www.ecoinvent.ch.
42 EERE (US DOE Energy Efficiency and Renewable Energy), Energy Intensity Indicators, 2013, web-accessed at http://www1.eere.energy.gov/ba/pba/intensityindicators/trend_data.html.
43 Kaeser, Kaeser Com-pak Blowers, Kaeser Refrigerated Air Driers, 2013, web-accessed at http://us.kaeser.com/Products_and_Solutions/.
44 J. E. Pope, *Rules of Thumb for Mechanical Engineers*, Gulf Publishing Company, Houston, 1997.
45 J. Koornneef, T. van Keulen, A. Faaij and W. Turkenburg, Life cycle assessment of a pulverized coal power plant with post-combustion capture, transport and storage of $CO_2$, *Int. J. Greenhouse Gas Control*, 2008, **2**(4), 448.
46 C. Yang and J. Ogden, Determining the lowest-cost hydrogen delivery mode, *Int. J. Hydrogen Energy*, 2007, **32**(2), 268.
47 M. S. Peters, K. D. Timmerhaus and R. E. West, *Plant Design and Economics for Chemical Engineers*, McGraw Hill, Boston, 2003.
48 Proton OnSite, *Hydrogen*, 2014. web-accessed at http://www.protononsite.com/.
49 EERE (US DOE Energy Efficiency and Renewable Energy), Saving energy, water, and money with efficient water treatment technologies, Technology Focus, DOE/EE-0294, 2004, web-accessed at http://www.nrel.gov/docs/fy04osti/34721.pdf.
50 J. Macknick, R. Newmark, G. Heath and K. C. Hallett, A Review of Operational Water Consumption and Withdrawal Factors for Electricity Generating Technologies, National Renewable Energy Laboratory, *Technical Report NREL/TP-6A20–50900*, 2011.
51 V. Fthenakis and H. C. Kim, Life-cycle uses of water in U.S. electricity generation, *Renewable Sustainable Energy Rev.*, 2010, **14**, 2039.
52 F. A. Mejia and J. Kleissl, Soiling losses for solar photovoltaic systems in California, *Sol. Energy*, 2013, **95**, 357.

53 A. K. Plappally and J. H. Lienhard, Energy requirements for water production, treatment, end use, reclamation, and disposal, *Renewable Sustainable Energy Rev.*, 2012, **16**, 4818.
54 FAO (Food and Agricultural Organization of the United Nations), Cost Control in Forest Harvesting and Road Construction, *FAO For. Dev. Pap.*, 1992, **99**. web-accessed at http://www.fao.org/docrep/T0579E/T0579E00.htm.
55 NREL (National Renewable Energy Laboratory), National Solar Radiation Data Base: 1991-2005 Update: Typical Meteorological Year 3, 2008, web-accessed at http://rredc.nrel.gov/solar/old_data/nsrdb/1991-2005/tmy3/.
56 G. Notton, C. Cristofari, M. Mattei and P. Poggi, Modelling of a double-glass photovoltaic module using finite-differences, *Appl. Therm. Eng.*, 2005, **25**, 2854.
57 W. Brutsaert, On a derivable formula for long-wave radiation from clear skies, *Water Resour. Res.*, 1975, **11**, 742.
58 M. Sugita and W. Brutsaert, Cloud effect in the estimation of instantaneous downward longwave radiation, *Water Resour. Res.*, 1993, **29**, 599.
59 S. Sharples and P. S. Charlesworth, Full scale measurements of wind-induced convective heat transfer from a roof-mounted flat plate solar collector, *Sol. Energy*, 1998, **62**, 69.
60 F. Incropera and D. DeWitt, *Fundamentals of Heat and Mass Transfer*, John Wiley and Sons, 5th edn, 2002.
61 T. Fujii and H. Imura, Natural-convection heat transfer from a plate with arbitrary inclination, *Int. J. Heat Mass Transfer*, 1972, **15**, 755.
62 K. Hassan and S. Mohamed, Natural convection from isothermal flat surfaces, *Int. J. Heat Mass Transfer*, 1970, **13**, 1873.
63 S. Armstrong and W. G. Hurley, A thermal model for photovoltaic panels under varying atmospheric conditions, *Appl. Therm. Eng.*, 2010, **30**, 1488.
64 NETL (National Energy Technology Laboratory), *Life Cycle Analysis: Power Studies Compilation Report, National Energy Technology Laboratory Report DOE/NETL-2010/1419*, 2010.
65 S. Ong, C. Campbell, P. Denholm, R. Margolis and G. Heath, *Land-Use Requirements for Solar Power Plants in the United States, National Renewable Energy Laboratory Report NREL/TP-6A20-56290*, 2013.
66 S. Hu, C. Xiang, S. Haussener, A. D. Berger and N. S. Lewis, An analysis of the optimal band gaps of light absorbers in integrated tandem photoelectrochemical water-splitting systems, *Energy Environ. Sci.*, 2013, **6**, 2984.
67 B. Seger, T. Pedersen, A. B. Laursen, P. C. K. Vesborg, O. Hansen and I. Chorkendorff, Using $TiO_2$ as a conductive protective layer for photocathodic $H_2$ evolution, *J. Am. Chem. Soc.*, 2013, **135**, 1057.
68 M. J. Kenney, M. Gong, Y. Li, J. Z. Wu, J. Feng, M. Lanza and H. Dai, High-performance silicon photoanodes passivated with ultrathin nickel films for water oxidation, *Science*, 2013, **342**, 836.
69 S. Hu, M. R. Shaner, J. A. Beardslee, M. Lichterman, B. S. Brunschwig and N. S. Lewis, Amorphous $TiO_2$ coatings stabilize Si, GaAs, and GaP photoanodes for efficient water oxidation, *Science*, 2014, **344**, 1005.
70 J. Peng, L. Lu and H. Yang, Review on life cycle assessment of energy payback and greenhouse gas emission of solar photovoltaic systems, *Renewable Sustainable Energy Rev.*, 2013, **19**, 255.
71 A. C. Goodrich, D. M. Powell, T. L. James, M. Woodhouse and T. Buonassisi, Assessing the drivers of regional trends in solar photovoltaic manufacturing, *Energy Environ. Sci.*, 2013, **6**, 2811.
72 J. S. Newman and K. E. Thomas-Alyea, *Electrochemical Systems*, ed. N. J. Hoboken, J. Wiley, 2004.
73 P. L. Spath and M. K. Mann, Life Cycle Assessment of Hydrogen Production *via* Natural Gas Steam Reforming, *NREL Technical Report NREL/TP-570–27637*, 2001.
74 D. J. Murphy, The implications of the declining energy return on investment of oil production, *Philos. Trans. R. Soc.*, 2014, **372**, 20130126.
75 A. K. Gupta and C. A. S. Hall, A review of the past and current state of EROI data, *Sustainability*, 2011, **3**, 1796.
76 D. Pimentel, Ethanol fuels: Energy balance, economics, and environmental impacts are negative, *Nat. Resour. Res.*, 2003, **12**(2), 127.
77 M. E. D. de Oliveira, B. E. Vaughan and E. J. J. Rykiel, Ethanol as fuel: Energy, carbon dioxide balances, and ecological footprint, *Bioscience*, 2005, **55**, 593.

 

*Energy & Environmental Science*

# Electronic Supplementary Information

## Life-cycle net energy assessment of large-scale hydrogen production via photoelectrochemical water splitting

Roger Sathre, Corinne D. Scown, William R. Morrow III, John C. Stevens, Ian D. Sharp, Joel W. Ager, Karl Walczak, Frances A. Houle, Jeffery B. Greenblatt

http://dx.doi.org/10.1039/C4EE01019A

## Tables

**Table S1.** Low, base-case, and high values of system model parameters. Low values result in reduced system performance relative to the base-case, while high values result in improved system performance.

| Parameter description | Units | Low | Base-case | High |
|---|---|---|---|---|
| **System** | | | | |
| Capacity factor of facility | percent | 80% | 90% | 95% |
| Primary energy-to-electricity conversion | percent | 40% | 50% | 60% |
| Life span of balance of system | years | 20 | 40 | 60 |
| Decommissioning energy | percent | 20% | 10% | 5% |
| **PEC cell** | | | | |
| Solar-to-hydrogen efficiency | percent | 5% | 10% | 20% |
| Life span of PEC cell | years | 5 | 10 | 20 |
| Cell degradation threshold | percent | 70% | 80% | 90% |
| Transmittance loss (dust, glass, electrolyte) | percent | 20% | 10% | 5% |
| Photo-active cell materials energy use | MJ $m^{-2}$ | 23 | 14 | 5 |
| Other cell materials energy use | MJ $m^{-2}$ | 1227 | 692 | 469 |
| Photo-active cell fabrication energy use | MJ $m^{-2}$ | 1668 | 1001 | 715 |
| Other cell fabrication energy use | MJ $m^{-2}$ | 517 | 407 | 359 |
| Electrolyte energy intensity | multiplier | 1.5 | 1.0 | 0.8 |
| **Panel** | | | | |
| Panel inactive area | percent | 10% | 5% | 2% |
| Panel material use | multiplier | 1.2 | 1.0 | 0.8 |
| Panel material energy intensity | multiplier | 1.2 | 1.0 | 0.8 |
| Panel internal frame spacing | meter | 0.5 | 1.0 | 1.5 |
| Panel transport (truck and train) | kilometer | 1300 | 300 | 0 |
| Containment vessel thickness | meter | 0.008 | 0.004 | 0.002 |
| Containment vessel material energy | multiplier | 1.5 | 1.0 | 0.8 |
| **Piping** | | | | |
| Maximum velocity, uncompressed H2 | m $sec^{-1}$ | 0.5 | 1.0 | 2.0 |
| Maximum velocity, compressed H2 | m $sec^{-1}$ | 20 | 40 | 60 |
| Maximum velocity, H2O | m $sec^{-1}$ | 1.0 | 3.0 | 5.0 |
| Material energy intensity | multiplier | 1.2 | 1.0 | 0.8 |
| Allowance for valves and fittings | percent | 50% | 25% | 10% |
| Pipe transport (train) | kilometer | 3000 | 1000 | 300 |
| **Gas handling** | | | | |
| Panels per blower | units | 50 | 100 | 150 |

| | | | | |
|---|---|---|---|---|
| Gas blower power | kW | 3.0 | 1.5 | 0.7 |
| Gas blower average use | percent of capacity | 100% | 75% | 50% |
| Gas dryer power | kW | 5.0 | 2.4 | 1.4 |
| Gas dryer average use | percent of capacity | 100% | 75% | 50% |
| Compressor specific energy use | W h $m^{-3}$ | 82 | 70 | 57 |
| Compressor interstage loss | psi | 10 | 5 | 0 |
| Gas intake temperature | degree C | 80 | 60 | 40 |
| Compressor fan load | percent | 10% | 7.5% | 5% |
| Gas handling hardware embodied energy | multiplier | 2.0 | 1.0 | 0.5 |
| **Storage** | | | | |
| Gas storage capacity | day | 2.0 | 1.0 | 0.5 |
| Allowable stress in tank wall | multiplier | 0.8 | 1.0 | 1.2 |
| Corrosion allowance | mm | 12 | 9 | 6 |
| Allowance for valves and fittings | percent | 20% | 10% | 5% |
| **Water** | | | | |
| Water treatment electricity | MJ $ton^{-1}$ of treated water | 43.1 | 21.5 | 16.1 |
| Water treatment brine waste | liter $ton^{-1}$ of treated water | 774 | 387 | 71 |
| Water use for panel cleaning | liter $m^{-2}$ $year^{-1}$ | 100 | 25 | 10 |
| Water transport electricity | kWh $m^{-3}$ $km^{-1}$ | 0.0073 | 0.0047 | 0.0018 |
| **Roads** | | | | |
| Road width | meter | 8 | 6 | 4 |
| Asphalt thickness | meter | 0.10 | 0.05 | 0.03 |
| Subbase thickness | meter | 0.30 | 0.15 | 0.08 |
| Percent bitumen in asphalt | percent | 6% | 5% | 4% |
| Material energy intensity | multiplier | 1.2 | 1.0 | 0.8 |
| **Operations** | | | | |
| Number of trucks and cranes | units | 12 | 6 | 3 |
| Horsepower of engines | brake hp | 600 | 400 | 200 |
| Daily operating time | hours | 24 | 12 | 8 |
| Equipment load factor | ratio | 0.70 | 0.54 | 0.38 |
| Panel heat requirement | kWh $m^{-2}$ $year^{-1}$ | 11.1 | 5.4 | 0.5 |

**Table S2.** Mass (kg) of panel components

| Component | Mass (kg) | Notes |
|---|---|---|
| Structure | 340 | Perimeter frame of steel channel section (ASTM C4x5.4), with internal elements of steel angle section (ASTM L2½x2x3/16) spaced at 1 m. |
| P5 piping | 7 | |
| PVC cell chamber | 163 | Based on Zhai *et al*. [28] |
| Glass cover | 207 | Based on Zhai *et al*. [28] |
| PEC cell elements | 4 | Based on Zhai *et al*. [28] |
| Electrolyte | 569 | 1M $H_2SO_4$, assume density of 1.045 kg $m^{-3}$ |
| Total | 1290 | |
| Total without electrolyte | 721 | |

**Table S3.** Characteristics of modeled PEC cells (Source: Zhai *et al.* [28])

| Category | Component | Lower case | Medium case | Higher case |
|---|---|---|---|---|
| Material choices | Photocathode | Silicon (Si) | Silicon (Si) | Silicon (Si) |
| | Photoanode | Tungsten trioxide ($WO_3$) | Tungsten trioxide ($WO_3$) | Gallium arsenide (GaAs) |
| | Catalysts for photocathode | Cobalt (Co) | Platinum (Pt) | Platinum (Pt) |
| | Catalysts for photoanode | No catalyst | No catalyst | Platinum (Pt) |
| | Encapsulation | Polyvinyl chloride (PVC) | Polyvinyl chloride (PVC) | Polycarbonate |
| | Thickness of chamber | 3 mm | 5 mm | 7 mm |
| | Thickness of membrane | 30 µm | 50 µm | 70 µm |
| Fabrication | Thermodynamic efficiency of processes used to fabricate photocathode/anode and membrane | 70% | 50% | 30% |

**Table S4.** Characteristics of base-case pipe levels P0 through P5 for $H_2$, $O_2$ and $H_2O$. Shaded pipe sizes are determined by minimum size (nominal ½ inch), not flow properties.

| | | P0 | P1 | P2 | P3 | P4 | P5 |
|---|---|---|---|---|---|---|---|
| **Length** | km | 300 | 15 | 144 | 1891 | 14385 | 21752 |
| **Maximum velocity** | m $sec^{-1}$ | | | | | | |
| H2 | | 40 | 40 | 40 | 1 | 1 | <<1 |
| O2 | | 40 | 40 | 40 | 1 | 1 | <<1 |
| H2O | | 3 | 3 | 3 | 3 | 3 | <<3 |
| **Flow rate** | kg $sec^{-1}$ | | | | | | |
| H2 | | 8.0 | 2.0 | 0.33 | 0.0045 | 0.00004 | << |
| O2 | | 63 | 16 | 2.6 | 0.035 | 0.00035 | << |
| H2O | | 142 | 18 | 3.0 | 0.040 | 0.00040 | << |
| **Pipe interior diameter** | inch | | | | | | |
| H2 | | 14 | 7.2 | 2.9 | 10 | 1.0 | 0.62 |
| O2 | | 10 | 5.1 | 2.1 | 7.3 | 0.73 | 0.62 |
| H2O | | 9.7 | 3.4 | 1.4 | 0.62 | 0.62 | 0.62 |
| **Pipe material** | | | | | | | |
| H2 | | PVC S80 | PVC S80 | PVC S80 | PVC S40 | PVC S40 | PVC S40 |
| O2 | | PVC S80 | PVC S80 | PVC S80 | PVC S40 | PVC S40 | PVC S40 |
| H2O | | PVC S40 | PVC S40 | PVC S40 | PVC S40 | PVC S40 | PVC S40 |

**Table S5.** Annual electricity requirement for panel heating to prevent freezing. The separate and combined effects of several possible design and operation conditions were assessed to estimate a likely range for the annual heating energy input. These were 1) to vary the minimum allowable temperature of the electrolyte from 0 °C to -2.5 °C; 2) to reduce the thermal radiation energy losses by reducing the emissivity of the window material from 0.94 to 0.8 using an optical coating; and 3) to add an additional 2 cm layer of R12 polystyrene insulation to the back of the device. Results indicate that variation of local climate has greater effect on panel heating energy than does variation of these conditions. The base-case conditions (shown in bold font in the table) assume a -2.5 °C temperature threshold, no insulation, and no low-emissivity coating.

| **Conditions** | | | **Heating energy (kWh $m^{-2}$ $year^{-1}$)** | | | |
|---|---|---|---|---|---|---|
| Temperature threshold | Insulation | Low-emissivity coating | Barstow | Phoenix | Las Vegas | Tucson |
| **-2.5 °C** | **none** | **none** | **11.0** | **0.6** | **6.1** | **4.2** |
| 0 °C | none | none | 23.9 | 3.1 | 16.1 | 14.0 |
| 0 °C | 2 cm R12 | none | 19.1 | 3.8 | 13.6 | 12.5 |
| 0 °C | none | top emissivity = 0.8 | 18.9 | 1.4 | 12.7 | 10.9 |
| -2.5 °C | none | top emissivity = 0.8 | 7.4 | 0.4 | 3.8 | 3.1 |

## Figures

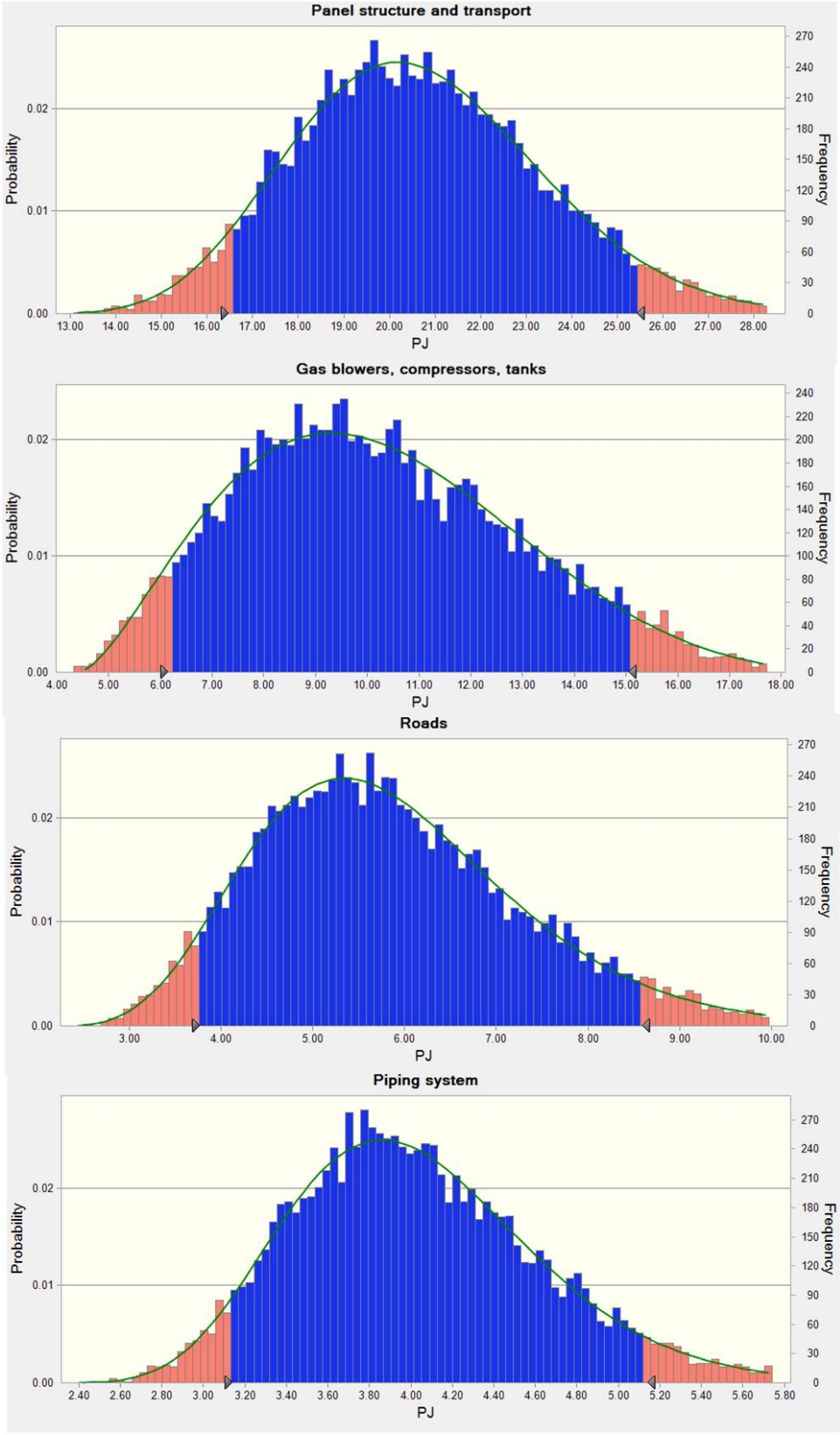
Panel structure and transport
Probability
Frequency
PJ
Gas blowers, compressors, tanks
Probability
Frequency
PJ
Roads
Probability
Frequency
PJ
Piping system
Probability
Frequency
PJ

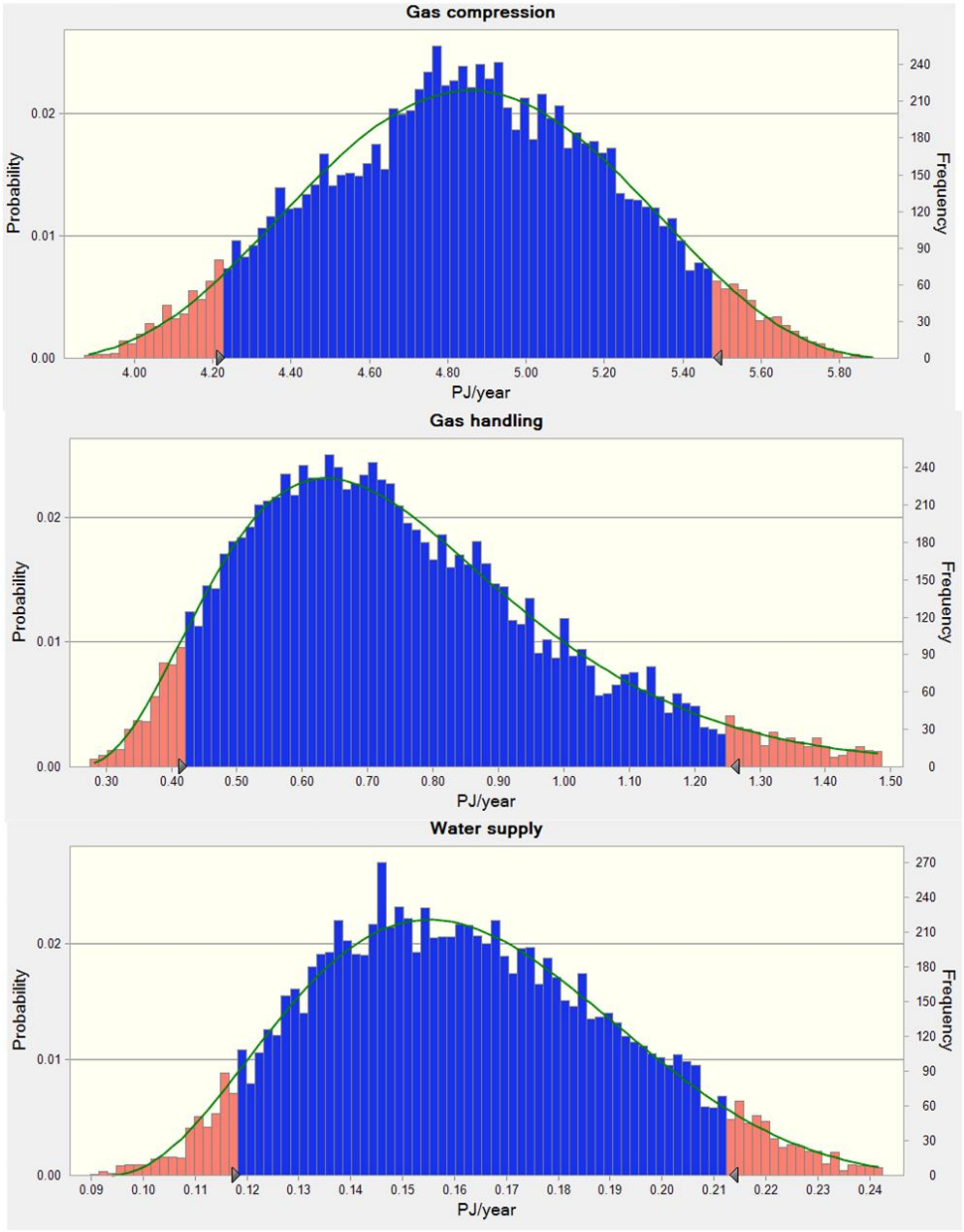


**Figure S1.** Outcomes of Monte Carlo simulations of parameter categories. Facility production energy use (top) is in units of PJ, and facility operation energy use (bottom) is in units of PJ year$^{-1}$.

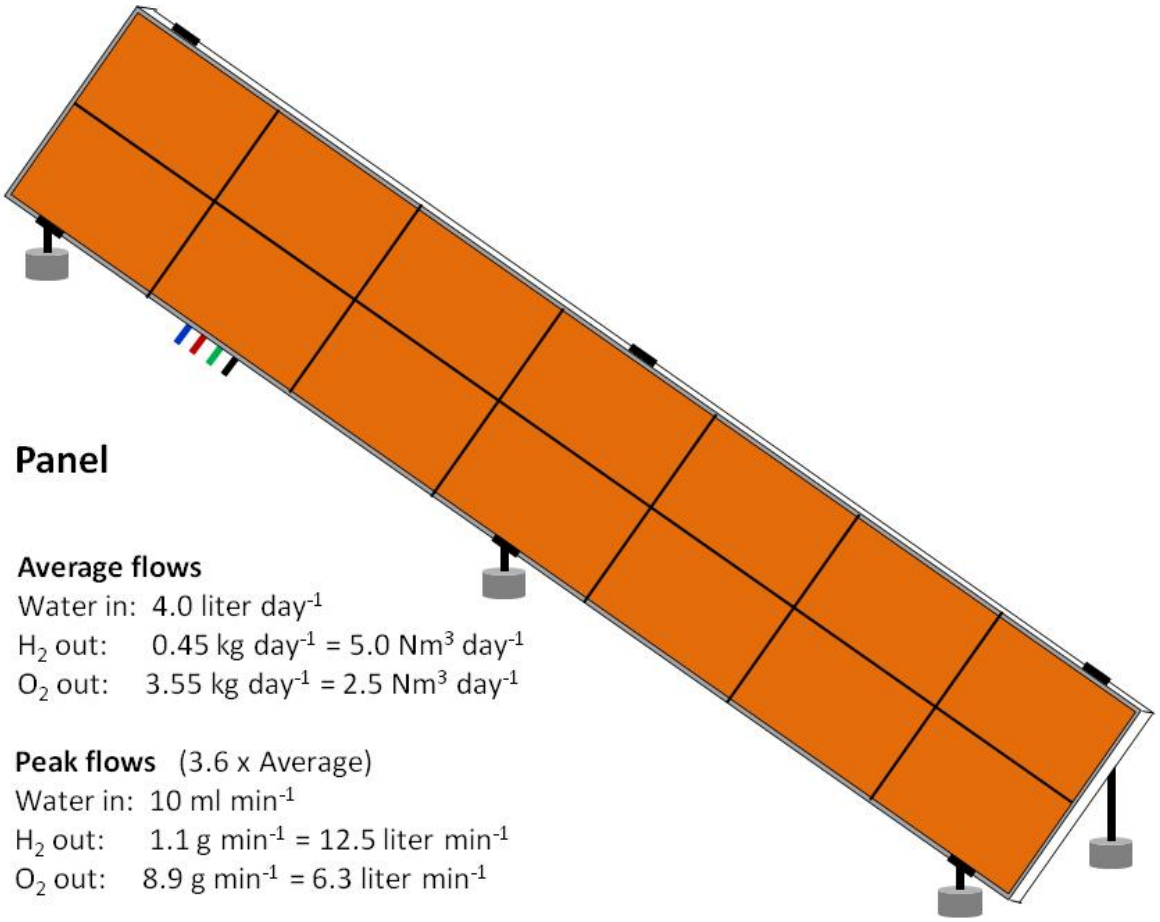


**Figure S2**. PEC panel with dimensions of 12.0 m long and 2.4 m wide. Flow rates are based on base-case conditions, and do not include water vapor lost with vented $O_2$.

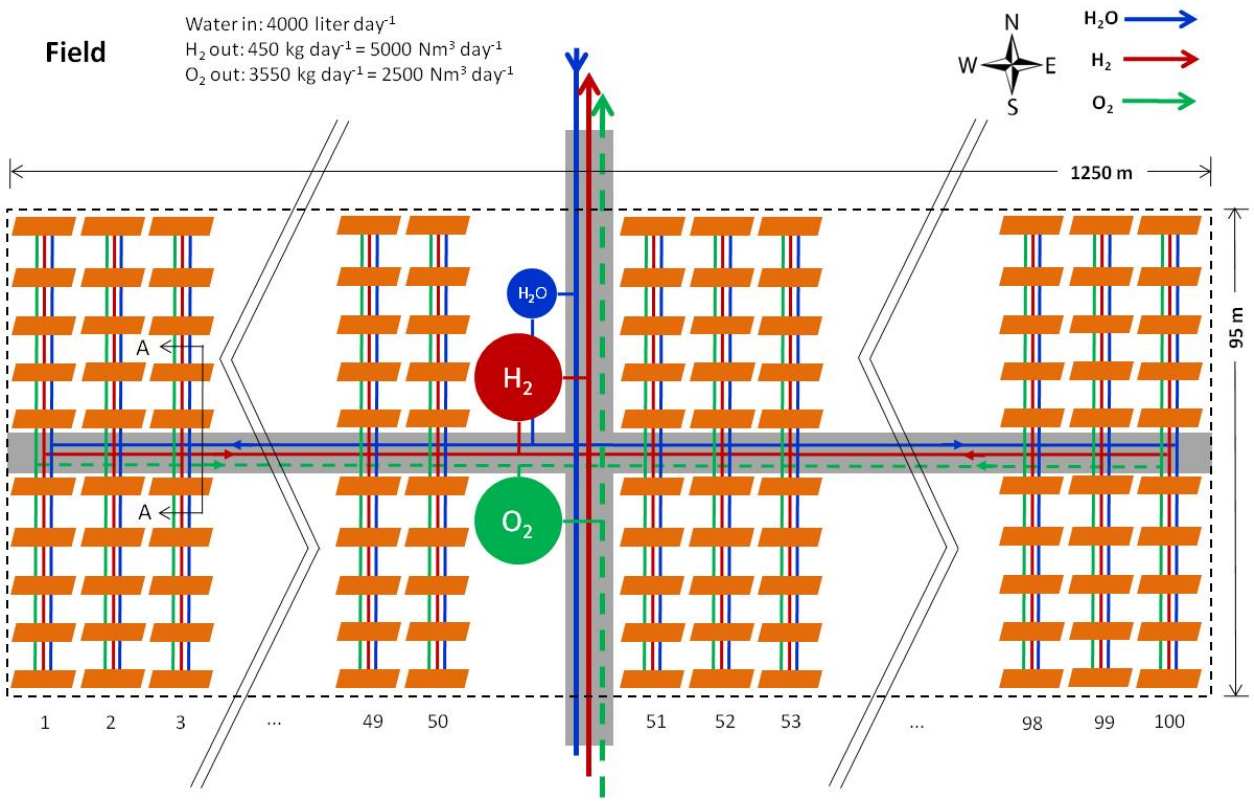


**Figure S3.** Diagram of a PEC field, comprising 1000 panels (100 rows of ten panels) plus compression and storage equipment for one day's production of $H_2$ (and $O_2$, if collected). Water flow rates do not include water vapor lost with vented $O_2$.

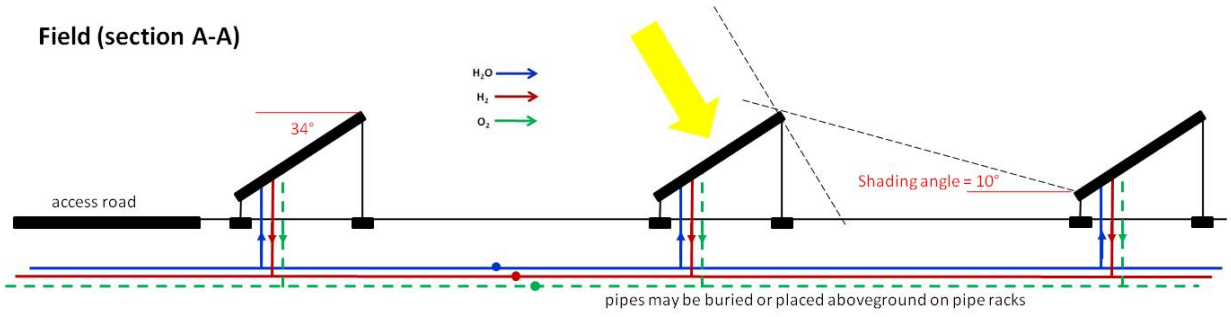


**Figure S4.** Cross sectional diagram of a PEC field, showing geometry of panel layout. Section A-A corresponds to indicator on Figure S3.

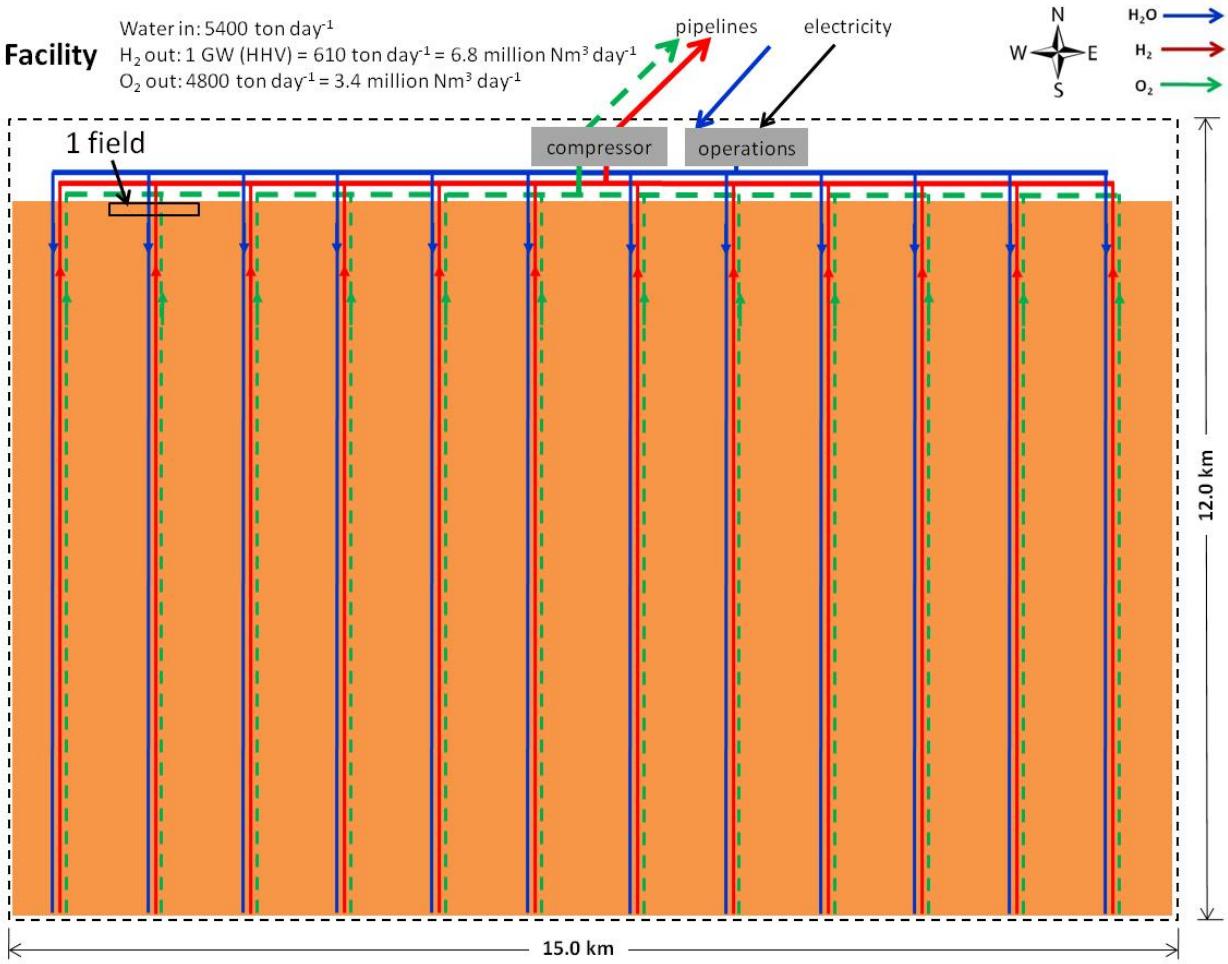


**Figure S5**. Diagram of PEC facility producing 1 GW (annual average) $H_2$. Water flow rates do not include water vapor lost with vented $O_2$.

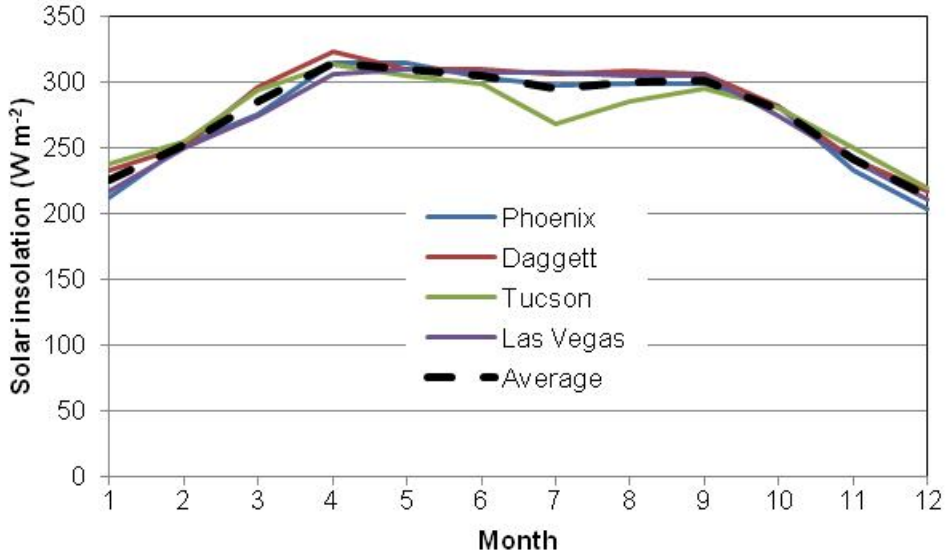


**Figure S6.** Monthly solar insolation (W $m^{-2}$) at four sites across the U.S. southwest. The assumed insolation on the facility is the average of the four sites, shown as a dashed line.

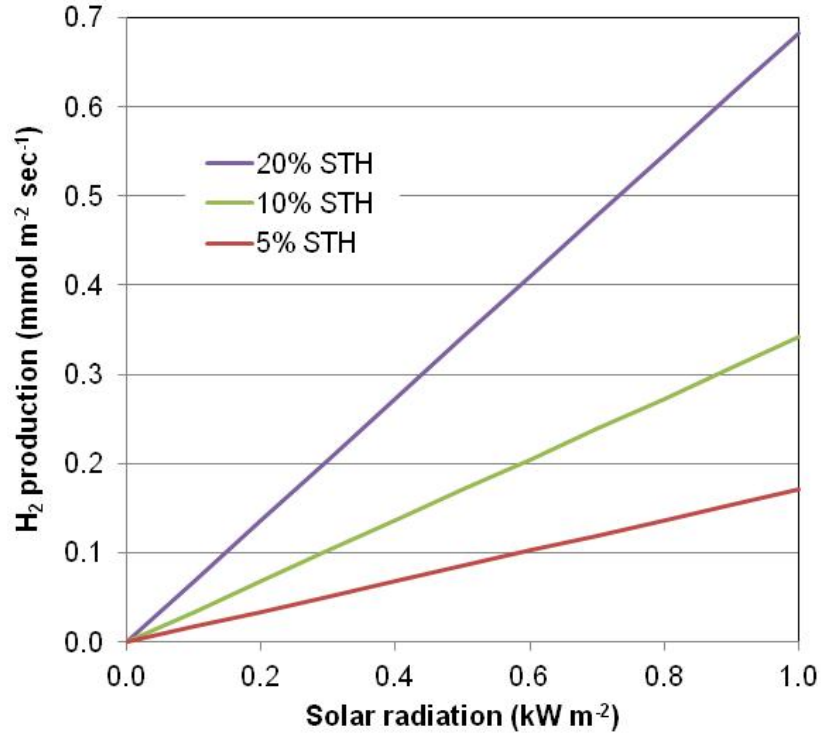


**Figure S7.** Assumed relation between instantaneous solar radiation and $H_2$ production.

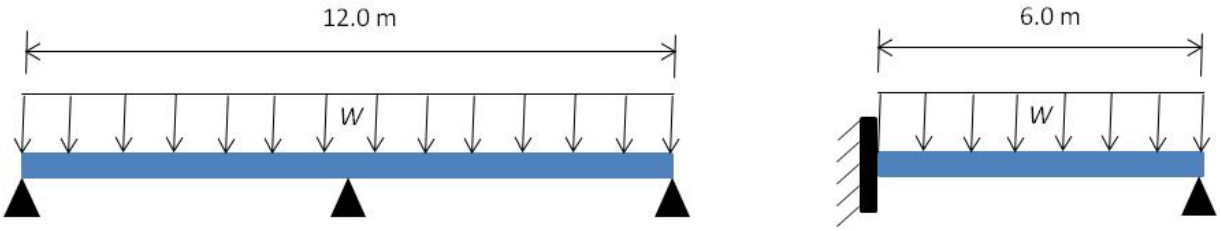


**Figure S8.** Estimation of panel deflection under load. Considering the panel as a uniformly-loaded beam that is simply supported at three points (left), symmetry implies that deflection will be equal to a beam fixed on one end and simply supported on the other (right). Based on Pope,[44] maximum deflection (inches) for such a beam will be:

$$y_{max} = \frac{-0.0054\, W\, L^4}{E\, I}$$

where W is the uniform load (pounds inch$^{-1}$), L is the length of the beam (inch), E is the modulus of elasticity of the material (psi), and I is the moment of inertia of the beam (inch$^4$). In this deflection analysis we assume the panel is laying flat; the uniform load is composed of the dead load of the steel structure (1.6 pounds inch$^{-1}$) plus the load of the PEC components and electrolyte (4.4 pounds inch$^{-1}$), to which is applied a safety factor multiplier of 3. The length of the (half) panel is 6.0 m or 237 inches. The modulus of elasticity of steel is about 3.1x10$^7$ psi. The moment of inertia of each of the two perimeter steel channel sections (ASTM C4x5.4) is 3.85 inch$^4$. These properties yield a maximum calculated deflection of 1.2 inches. The calculated length-to-deflection ratio is about 190, which is marginally acceptable for typical structural solutions. There appears to be significant scope for increasing material use efficiency through creative design that integrates PEC cell materials into a structural solution.

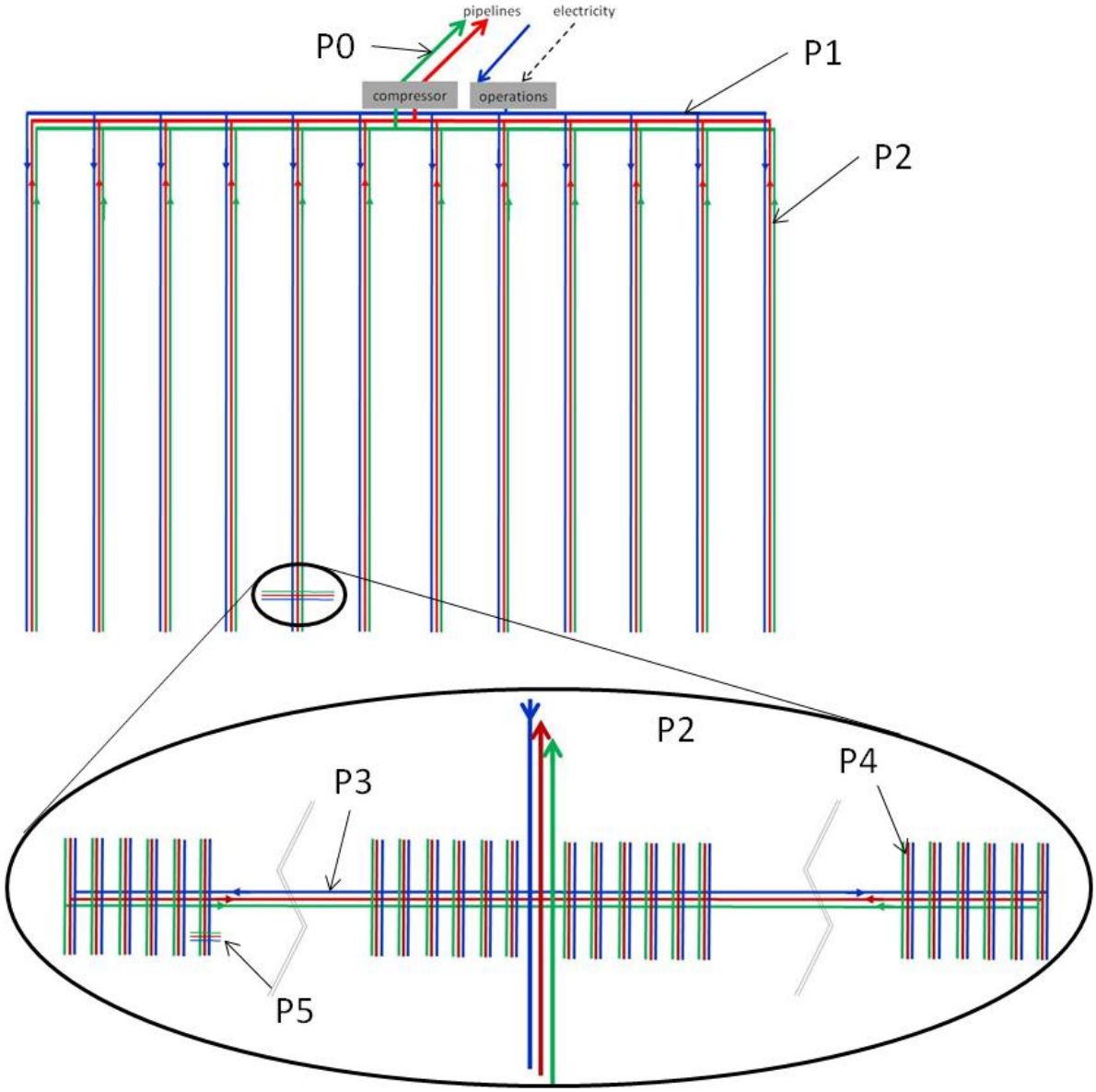


**Figure S9.** Hierarchical piping networks to transport fluids. Water, hydrogen and oxygen conduits are represented by blue, red and green lines, respectively.

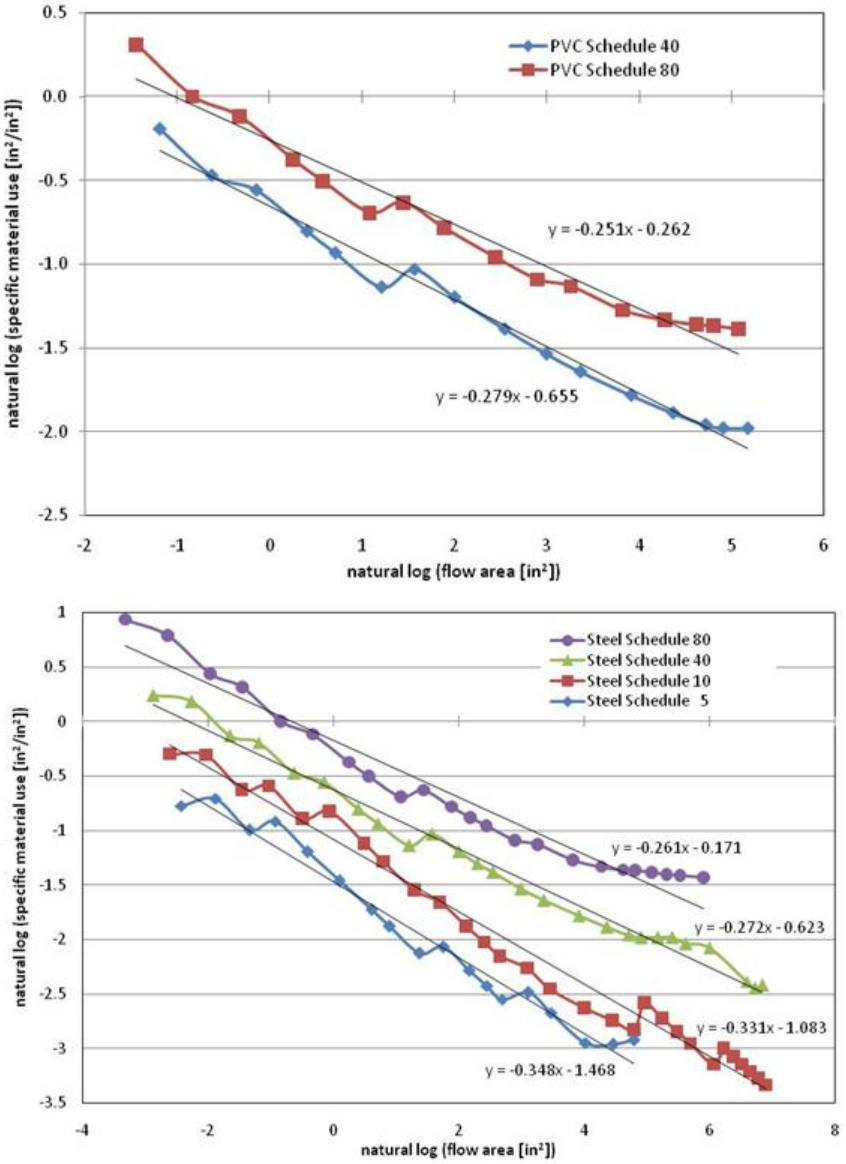


**Figure S10.** Relation between the flow area and specific material use of standard sizes of pipes made of PVC (top) and steel (bottom). Pipe dimensions are based on open-source data reporting agreed standards, namely ASTM D1785 (Poly Vinyl Chloride Plastic Pipe) and ASME B36.10 (Welded and Seamless Wrought Steel Pipe). Pipe sizing in this analysis is based on the fit lines.

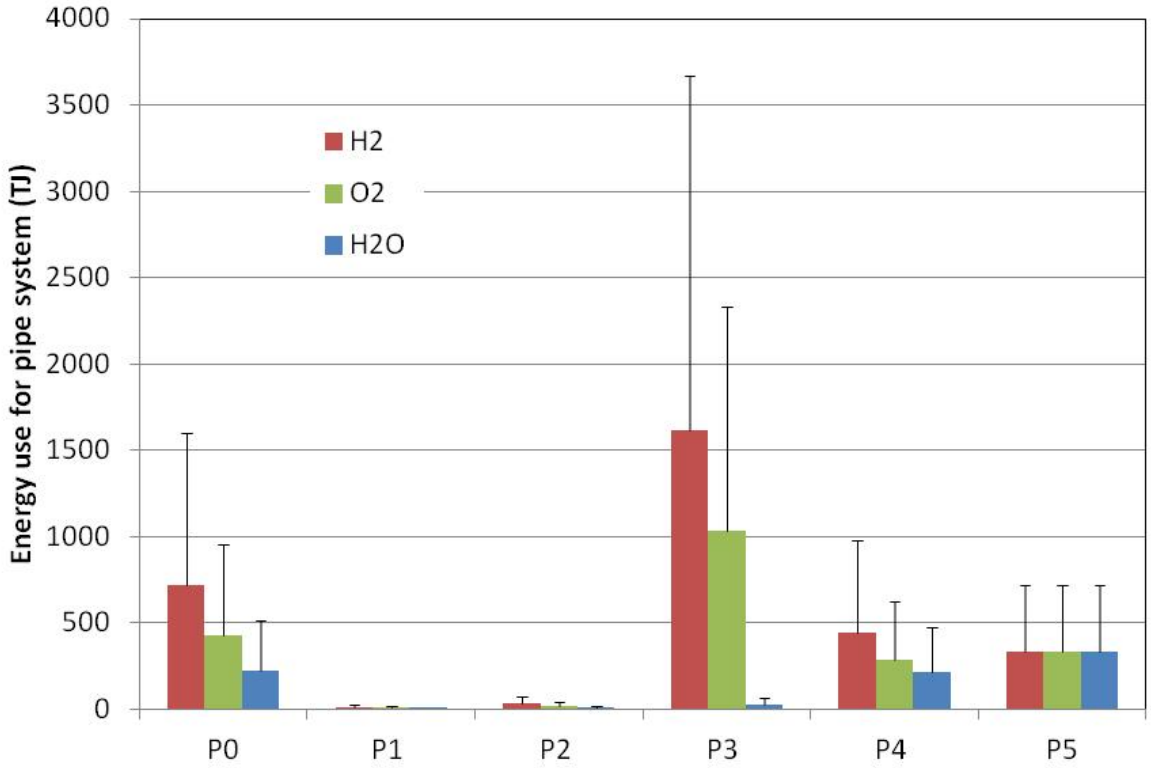


**Figure S11.** Energy use for production of piping system for the gas and liquid flows in the facility ($H_2O$, $H_2$, $O_2$). Colored bars show energy use for base case PVC pipes, error bars show additional energy use for steel pipes.

## Details of $H_2$ demand scenarios

Light-duty vehicle travel demand in 2014 is approximately 2.70 trillion miles (EIA 2014). Based on NRC (2013), we assume that average light-duty vehicle hydrogen fuel cell efficiency is 13.5 kg $H_2$ per 1000 miles (based on the average of passenger car and light truck efficiencies), roughly 3.5 times more efficient than conventional gasoline engines. This results in an annual demand of 35.4 billion kg $H_2$. Assuming each 1 GW facility produces 222 million kg $H_2$ per year, 160 such facilities would be required. By 2050, NRC (2013) projects average fuel cell efficiency will decrease fuel consumption to 7.5 kg $H_2$ per 1000 miles, while we project travel demand will increase to 3.76 trillion miles (based on extrapolation of EIA projections through 2040). These combined changes result in a 2050 demand of 28.2 billion kg $H_2$, requiring 127 1 GW facilities to produce it.

EIA (US Energy Information Agency), *Annual Energy Outlook 2014 Early Release*, 2014. Web-accessed at http://www.eia.gov/forecasts/aeo/er/index.cfm

National Research Council, *Transitions to Alternative Vehicles and Fuels*, Washington, DC: The National Academies Press, 2013. Web-accessed at http://www.nap.edu/catalog.php?record_id=18264